Thesis

Electronic States in Two-Dimensional Lattices under Strong Electric Fields

Takeshi Nakanishi

Department of Physics
Osaka University

1995 January

Acknowledgments

The author is grateful to Professor Motohiko Saitoh, who introduced the author to this field of research, and for critical reading of the manuscript. He would like to express his sincere thanks to Dr. Tomi Ohtsuki for valuable discussions with him and for his critical reading of the manuscript. He would also like to record his warmest acknowledgements to Professor Hiroshi Matsukawa and Dr. Yoshifumi Sakamoto for many valuable discussions. I would like to thank to Professor M. Saitoh, H, Akai, Y, Akutsu, K. Murase and H. Matsukawa for their troubling themselves to hold an inquiry into the present thesis. He acknowledges the financial support from the Research Fellowships of the Japan Society for the Promotion of Science for Young Scientists. He would like to thank Dr. Takeshi Kurimoto and the administrators of ODINS for preparing the environment for his numerical calculations.

Abstract

The electronic states of the two–dimensional tight–binding model in the strong electric field are investigated. The electronic states of the one–dimensional tight–binding model in the strong electric field is called Stark ladder states, which are characterized by the evenly spaced energy levels and localized wavefunctions. Numerical solutions for eigenenergies and eigenfunctions are presented as functions of the angle between the electric field and the symmetry axis of the lattice. We show the existence of the Stark ladder states in the two–dimensional tight–binding lattice. Unexpected gaps open near the band edges for appropriate electric fields, the magnitudes and the positions of which are smooth functions of the angle for a fixed electric field. The effects of the system edges are also discussed.

The electronic states of the two–dimensional system applied the electric field in the plane and a magnetic field normal to it are also studied. The magnetic subbands at zero electric field are modified by the electric field. It is discussed whether or not the eigenenergies for high electric fields are represented by the Stark ladder states associated with each of the magnetic subbands. When the electric potential drop across the system becomes comparable to the bandwidth of zero electric and magnetic fields, the density of states becomes the pyramid shape with steps, the steps being induced by the finiteness of the lattice. The influence on the eigenenergies by the change of the direction of the electric field is also discussed.

The nature of the ballistic transport properties of this system is investigated. The electric field makes the electron wave functions localized in the parallel direction to the electric field while they are plane wave like in the perpendicular direction, producing narrow channels perpendicular to the electric field. Numerical computations are performed on the basis of the two-terminal Landauer formula for the conductance

with the transmission coefficients calculated by the recursive Green's function technique. The dependence on the magnetic field and random potentials is calculated.

Contents

List of Figures

Chapter 1

Introduction

A history to understand Bloch electron in the electric and magnetic field is reviewed. When the strong electric field is applied to the periodic system, the Stark ladder states are formed, which are characterized by the evenly spaced energy levels and localized wavefunctions. We attempt to survey the Stark ladder by using a semi–classical and quantum treatment. We also review the Harper model which is the two dimensional tight–binding model in the magnetic field.

1.1 Stark ladder States

Homogeneous external electric fields must have a very peculiar relationship to the energy bands of a Bloch particle. The notion is followed up for the case of the one dimensional systems [1]. If we suppose that there is no interband coupling and the particle is confined to one band only, it is concluded that the wavefunction is localized in the width $W_0 a/2\mathcal{E}$ along the electric field direction, where W_0 is the bandwidth at zero electric field, $\mathcal{E}$ the electric field and a the lattice constant, and the eigenvalue is given by

$$E_\nu = F\nu, \tag{1.1}$$

where $F = e\mathcal{E}a$ is the electric potential drop across a unit cell and ν an integer. The eigenvalue with even spacing F is different qualitatively from continuous spectrum of the zero electric field case. This is called "Stark ladder" by Wannier [2,3].

Recently, several experiments [4,5] have confirmed various aspects of the Stark ladder in GaAs–AlGaAs superlattices where the period of the potential and the bandwidth are artificially tunable. This effect attracted a lot of attention due to not only the evidence of the Bloch oscillation but also the application side of an electro–optical switch utilizing the blue shift.

In the following we attempt a theoretical survey of the Stark ladder. Efforts will be made to provide a comparison between the fully quantum mechanical treatment and the semiclassical one.

In the semiclassical treatment within a band the particle moves according to the "Newton" law

$$\hbar\frac{dk}{d\tau} = -e\mathcal{E}, \tag{1.2}$$

where τ is the time. From this equation, we get

$$k(\tau) = k_0 - e\mathcal{E}\tau/\hbar. \tag{1.3}$$

The semiclassical equations of motion are entirely determined when Eq. (1.2) is used in conjunction with the definition of the velocity for a semiclassical electron

$$v = \frac{1}{\hbar}\frac{\partial\epsilon(k_0 - e\mathcal{E}\tau/\hbar)}{\partial k}, \tag{1.4}$$

where $\epsilon(k)$ is the dispersion relation in the absence of the external electric field. v and thus the position x are periodic functions of time with a period T_B equal to

$$T_B = 2\pi\hbar/e\mathcal{E}a = 2\pi/\omega_B, \tag{1.5}$$

since $\epsilon(k)$ is periodic in k with periodicity $2\pi/a$. The oscillatory motion described by Eqs. (1.4) and (1.5) is the Bloch oscillation, and $\omega_B = F/\hbar$ is the Bloch angular frequency.

The quantum treatment of this problem, restricting ourselves to a one–band tight–binding model [6,7], is described by the following Schrödinger equation,

$$t\{C(x+1) + C(x-1)\} + FC(x) = EC(x), \tag{1.6}$$

where t is the transfer integral between the nearest neighbor sites and the units are chosen such that the lattice constant a is unity. It has been shown by Katsura, Hatta and Morita [6] that the wavefunction of Eq. (1.6) is represented by the Bessel function

$$C(x) = J_{x-\nu}(2t/F), \tag{1.7}$$

with the energy eigenvalue given by Eq. (1.1). The spacing between two consecutive eigenvalues is $\hbar\omega_B$. These quantized energy levels originate from the periodicity of the lattice. Subsequently, Kane [8] constructed the wavefunction by the superposition

of the Bloch wavefunctions for a general shape of a band, and has obtained exactly the same spectra as Eq. (1.1). The obtained wavefunctions show a similar behavior to the one in the tight-binding model(1.7), and are spatially localized, which one could have anticipated from the semiclassical result, within the length of the order of

$$\lambda = 2t/F. \tag{1.8}$$

The Stark ladder representation may fail when F is so small that λ exceeds the crystal length L (scaled by a) [9]. Eq. (1.1), should be a good description when the potential drop through the crystal, $V = FL$, satisfies the condition

$$V \gg W_0, \tag{1.9}$$

where $W_0 = 2t$ is the bandwidth for the zero field.

It is remarkable that the spectrum (1.1) and wavefunction (1.7) of the Stark ladder states are very different from those of the Bloch states: in the former the energy spectra are discrete and the wavefunctions are localized, while they are continuous and extended in the latter. These contrasted characters occur in an infinite lattice, where the electric field potential is unbounded even for an infinitesimally small electric field and $F = 0$ is a singular point of the energy spectra.

In order to see the change from the Bloch states to the Stark ladder states, it is thus necessary to examine the lattice of finite size, where the electric potential drop through the system is finite. The energy spectrum of the finite linear chain is investigated by Stey and Gusman [10] and Saitoh [11]. Indeed, the change from the Bloch states to the Stark ladder states is smooth as a function of the electric field, and in an intermediate field strength, there appear the Airy edge states, in which

the wavefunctions are characterized by the Airy functions

$$C_i(x) = 2\pi \left(\frac{F}{t}\right)^{1/3} \mathrm{Ai}\left[\left(\frac{F}{t}\right)^{1/3} x + Z_i\right], \tag{1.10}$$

and the corresponding eigenenergy is represented by

$$E_i = -2t + |Z_i|(t\,F^2)^{1/3}, \tag{1.11}$$

where Z_i is the i–th zero of the Airy function.

On the experimental side, the search for Stark ladders proved to be elusive, although there have been reports on their indirect observation in the early 1970s in a cubic ZnS [12] and wide–band–gap semiconductors [13]. Maekawa [12] found a stepwise increase of the electrical conductivity as a function of electric field. These results were theoretically analyzed by Saitoh [14]. Other experimental support [13] for the existence of the Stark ladder has been given in the optical absorption study by Koss and Lambert, although, as these authors pointed out, the experimental uncertainty is rather large. Actually, the dominant effect of an electric field on the absorption edge of a bulk semiconductor is the appearance of the Franz–Keldysh effect [15,16], *i.e.*, the optical–absorption coefficient exhibits a tail below the edge of $F = 0$ with an oscillatory behavior above there. These effects originate from the field–induced breakdown of the optical selection rules($\Delta k = 0$) along the electric field. In addition, for bulk samples, it was quickly realized that the time needed to complete a period of the semiclassical bound motion was considerably longer than any realistic collision time due to impurities, defects, phonons, and so on, thus leaving only a faint hope for observing this effect clearly.

Recently, due to the recent improvement of the epitaxial techniques, artificial semiconductor heterostructures are realized [17]. For example, superlattices are prepared by stacking GaAs layer and AlGaAs layer alternately and have the artificial

periodic potential along the growth axis. The superlattices consist of a series of quantum wells coupled by the resonant tunnelling effect. They are unique systems where the bandwidth can be controlled in the range of a few tens of meV. This bandwidth is narrow enough for the condition (1.9) to be satisfied for moderate electric fields in the range of a few tens of kV/cm and the high–field limit can be explored. This narrow band is called miniband which is due to the long period of artificial potential with the period of which is of the order of μm. Due to the long period, the wavefunction is expected to be localized in one well for the extremely strong electric field case. Note that this expected character is different from the case of the uniform semiconductor sample which is mentioned before, where the wavefunction is extended on the hundred or more atoms. Thus, Voisin suggested a reexamination of the Stark problem in semiconductor superlattices from the point of view of the inhibition of the resonant tunnel effect between consecutive wells. For such systems as the field is increased, the system is expected to behave more and more like a series of uncoupled quantum wells, and its optical–absorption line shape evolves from the miniband profile at $F = 0$ to a step function [4] at large field, showing a blue shift [18] of the absorption edge of the order of half the sum of the conduction and valence miniband widths. Mendez *et al* [18]. and Voisin *et al.* [5] experimentally demonstrated the existence of a blue shift in GaAs–AlGaAs superlattices. Since then, several experiments have confirmed various aspects of the Stark ladder [19], including a room temperature achievement of an electrooptical switch utilizing the blue shift [20].

In the above discussion we suppose that there is no interband coupling and the particle is confined to one band only. When the potential drop through the system V becomes greater than the bandgap we must take into account the modification

due to other bands. It has been discussed extensively whether or not the existence of another band destroys the Stark ladder [14,21–28]. It is confirmed theoretically that the Stark ladder exists within the multi–band tight–binding models [22,23,28]. In the experimental side the Stark ladder effect is confirmed in the high field, where level of one band is made to anticross another level belonging to another band, as demonstrated and analyzed by Schneider *et al.* [29], Nakayama *et al.* [30] and Bastard *et al.* [31]. Even if the electric field becomes extremely strong such as the energy level belonging to the band of which wavefunction is localized in the well is equal to one belonging to the next band of which wavefunction is localized in the next well, the resonant couplings between the Stark localized states of minibands in the electroreflectance measurement is observed [32].

When two–dimensional systems are considered, another complexity arises due to the freedom of the direction of the electric field with respect to the symmetry axis of the lattice. When the direction of the electric field is $[M, N]$, where M and N are mutually prime each other and $M\,N\ \neq 0$, the periodicity along the field direction is an irregular function of the angle between the field and the [1 0] direction, and in the irrational direction, *i.e.*, when the tangent of the angle is irrational, the periodicity length can not be defined. We must study to answer the question whether or not the physically observable quantity such as the density of states is a smooth function of the angle. It is also interesting to see how the edge states which is described by the Airy function in one–dimension case as mentioned before, are modified in two–dimensions.

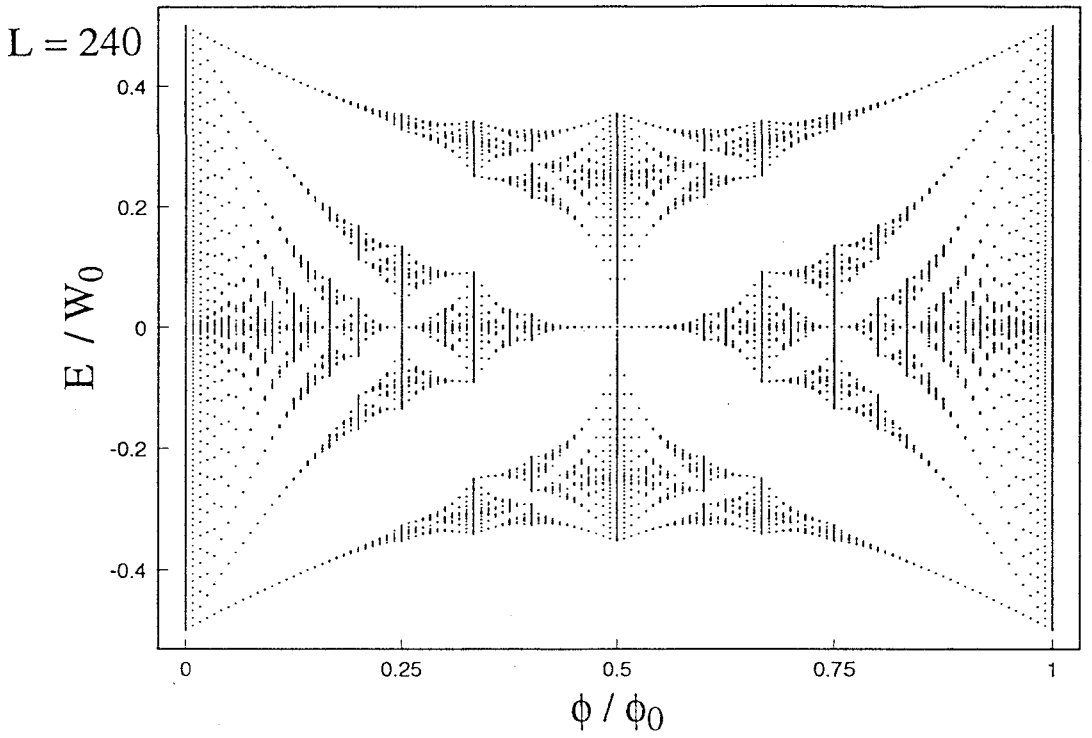

Figure 1.1: Eigenenergies E/t is plotted against the normalized magnetic flux ϕ/ϕ_0. The eigenenergies are calculated by the numerical diagonalization on the system of which dimension $L = 240$.

1.2 Electronic States of the two–dimensional tight–binding model in the Magnetic Field

When an electric field is switched off and only a magnetic field is applied perpendicular to the lattice, it is known that the electronic spectrum of a two–dimensional tight–binding model shows a fairly complicated behavior [33–35], as shown in Fig. 1.1, where E is plotted against the magnetic flux ϕ in units of the flux quanta $\phi_0 = ch/e$. The structure often called the Hofstadter butterfly is characterized by the recursive structure, and by multiple magnetic subbands with gaps induced by the magnetic field [33,36]. This model is studied in several papers [37–40] as a trial towards the understanding of the quantized Hall effect [41].

An effective single-band Hamiltonian representing a crystal electron in a uniform magnetic field is constructed from the tight-binding form of the Bloch band by replacing $\hbar\mathrm{k}$ by the operator $\mathbf{p} + e\mathbf{A}/c$, where $\mathbf{A}$ is the vector potential [42]. Work to justify this substitution has been done [2,43–45]. This substitution is possible as long as we assume that the magnetic fields are weak enough so that we may neglect contributions from different bands and that the magnetic fields are not too rapidly varying.† By taking the Landau gauge for the vector potential:

$$\mathbf{A} = B(0, x), \tag{1.12}$$

the Hamiltonian is given by

$$H = -t \sum_{x,y} \left[a^{\dagger}_{x+1,y} a_{x,y} + a^{\dagger}_{x,y+1} a_{x,y} \mathrm{e}^{-i2\pi(\phi/\phi_0)x} + h.c. \right], \tag{1.13}$$

where $a^{\dagger}_{x,y}(a_{x,y})$ creates (annihilates) an electron at site (x, y) and t the transfer integral between nearest neighbor sites. We restrict ourselves to the case of rational flux, *i.e.*, $\phi = Ba^2 = (p/q)\phi_0$ where p and q are mutually prime integers each other. If the periodic boundary conditions are imposed along the y direction

$$C(x, y) = C(x, y + L), \tag{1.14}$$

and the wavefunction is Fourier transformed with respect to y,

$$C_x(k) = \frac{1}{L} \sum_{m=0}^{L} \mathrm{e}^{iky} C(x, y), \tag{1.15}$$

where

$$k = 2\pi m/L - \pi, \quad (m = 0, 1, \cdots, L-1), \tag{1.16}$$

then the Schrödinger equation leads

$$-t\left[C_{x+1}(k) + C_{x-1}(k)\right] + V(x)C_x(k) = EC_x(k), \tag{1.17}$$

†In our case these conditions are satisfied because we consider the uniform magnetic field and for fields $B \sim 10^4$ oersteds and taking $a \sim 10^{-8}$ cm the Landau level separation is order of the 10^{-4} compared to the bandwidth [46].

where k is the wave vector along the y direction and

$$V(x) = \Lambda t \cos(2\pi \frac{p}{q} x + k), \tag{1.18}$$

with $\Lambda = 2$ which is used for later reference. This equation is sometimes called Harper's equation [46] and has been studied by a number of authors [33,36,47]. As the potential $V(x)$ in Eq. (1.17) satisfies

$$V(x) = V(x + q), \tag{1.19}$$

the magnetic unit cell is defined as stacked q original unit cell in the x direction. The eigenvalue of Eq. (1.17) is studied by Azbel [36] and later numerically solved by Hofstadter [33] as shown in Fig. 1.1. Only rational value of p/q with interval $1/60$ are shown in the figure. The spectrum is divided into q magnetic subbands with gaps in between. When ϕ is the irrational multiple of the flux quantum, it has been pointed out that the spectrum is uncountable but measure–zero set of points. This is also related to the one dimensional system in the quasi periodic potential [48–50].

The properties of the wavefunction $C_x(k)$ also have been well understood. The duality arguments suggest that for $\Lambda < 2$ all the states should be extended while they are localized in the x direction for $\Lambda > 2$. At $\Lambda = 2$ all states are critical [51].

When both the electric and magnetic fields are present [3,26,52,53], the question arises whether or not the gaps induced by the magnetic field remain stable and how the energy spectrum is modified. It is expected in the strong electric field that the character of wave functions may change from the Landau type to the Stark ladder one. Wannier *et al.* [2,3] discussed the possibility of handling the system under both electric and magnetic fields in a infinite solid. In the real system, however, the system boundaries have to be taken into account in the calculation of the energy spectrum. Claro *et al.* [52] studied this problem numerically, where they used the

single mode of sinusoidal potential due to the periodic potential and ignored Landau–level mixing. It is not trivial, however, to answer the question whether or not the effect of other magnetic subbands is negligible, especially for the neighboring bands of the small gaps as shown in Fig. 1.1. Note that in the case of the tight–binding model, the Landau–level is seen as the magnetic subbands for the weak magnetic field near the band edge. Niu [26] studied the one dimensional tight–binding model in the electric and periodic potential and showed the system is characterized by q sets of Stark ladder, for the case $\Lambda \ll 2$ in Eqs. (1.17) and (1.18). However the accurate calculation for the two–dimensional tight–binding model of a finite system in applied by the electric field in the plane and magnetic fields normal to it has never done. Thus we calculate in this thesis the eigenvalues and eigenstates of it by the numerical diagonalization.

1.3 Quantum Dot Lattice

The model system may be realizable in the quantum dot lattices [54] made of semiconductors, in which the lattice spacing is controllable, and the strong field condition considered in this thesis may be fulfilled easily by experimentally accessible field strengths. The quantum dot lattice is realized by the progress of techniques of lithography and etching techniques. It is possible to confine laterally quasi–two–dimensional electron gases at semiconductor interfaces into dots of diameter less than the mean free path of electrons at low temperatures. The sample has a MOS (metal–oxide–semiconductor systems) capacitor with a cross–grated NiCr evaporated onto the InSb substrate. At the interface between NiCr and InSb a Schottky contact is established and the Fermi energy E_F is pinned within the band gap. Under the small dot areas where there is no metal on the InSb surface, mobile electrons can be induced by the gate voltage since the InSb substrate has a finite resistivity even at liquid helium temperatures. In the above structure there is no tunneling between adjacent dots since the barrier between dots is high and barrier width is long $\sim$ 150nm. Thus this sample is inadequate for our purpose. We need the dots lattice with low barrier and short periodicity of them for electrons to be able to tunnel between dots so that the mini–bands are made. Such suitable sample has not been realized yet as far as the author knows, and thus the more improvement of the techniques is necessary for realization of the model considered in this work.

1.4 Organization of This Thesis

The organization of this thesis is as follows. In the following chapter, we discuss the electronic states and wavefunctions of the two dimensional tight-binding model in the electric field. We calculate them numerically by diagonalization and the density of states are presented as functions of the angle between the electric field and the symmetry axis of the lattice. Unexpected gaps open near the band edges for appropriate electric fields, the magnitudes and the positions of which are smooth functions of the angle for a fixed electric field. The effects of the system edges are also discussed.

In Chapter 3, the electronic states of the two-dimensional tight-binding model when the electric field is applied in the plane and magnetic field normal to it are studied. The magnetic subbands in the absence of the electric field are modified by the presence of the electric field and it is discussed whether or not the eigenenergies for high electric fields are represented by the Stark ladder states associated with each of the magnetic subbands. The influence on the density of states by the change of the direction of the electric field is also discussed.

In Chapter 4, the nature of the ballistic transport properties of the two-dimensional lattice in the strong electric fields is investigated. Combination of the electric and magnetic fields makes the electron wave functions localized in the electric field direction which is considered as the narrow channels perpendicular to the electric field. Numerical computations are performed on the basis of the two-terminal Landauer formula for the conductance on the narrow channel with the transmission coefficients calculated from the recursive Green's function technique. The magnetic field and random potential dependence is calculated. The final chapter is devoted to summary and concluding remarks.

Chapter 2

Stark Ladders in a Two–Dimensional Tight–Binding Lattice

In this chapter the electronic states of a two–dimensional tight–binding model in a uniform electric field are studied. Numerical solutions for eigenenergies and eigenfunctions are presented as functions of the angle between the electric field and the symmetry axis of the lattice. When the direction of the electric field is $[M, N]$, where M and N are mutually prime each other and $M\,N \neq 0$, the eigenenergies are shown to be quantized with an interval equal to the potential drop between the nearest neighbor equi–potential lines. Though the level separation varies discontinuously with the change of the direction, the smeared out density of states is shown to be independent of the direction of the electric field, except for the direction [1 0] where the motions parallel and perpendicular to the electric field directions are separable. Unexpected gaps open near the band edges for appropriate electric fields, the magnitudes and the positions of which are smooth functions of the angle for a fixed electric field.

2.1 Introduction to Chapter 2

The electronic energy spectra in a periodic potential in an electric field have been studied extensively [1,2,6,8]. In a one-dimensional single-band tight-binding model, it has been shown by Katsura, Hatta and Morita [6] that the wavefunction is represented by the Bessel function and the energy spectra are quantized with the separation of the electric potential drop F across a unit cell. These quantized energy levels originate from the periodicity of the lattice and are called Stark ladders by Wannier [2].

It is remarkable that the characters of the Stark ladder states are very different from the Bloch states: in the former the energy spectra are discrete and the wavefunctions are localized, while they are continuous and extended in the latter. These contrasted characters occur in an infinite lattice, where the electric field potential is unbounded even for an infinitesimally small electric field and $F = 0$ is a singular point of the energy spectra.

In order to see the transition from the Bloch states to the Stark ladder states, it is necessary to examine the lattice of finite size, where the electric potential drop through the system is finite. The energy spectrum of the finite linear chain is investigated by Stey and Gusman [10] and Saitoh [11], in which the wavefunction is characterized by the Airy type wavefunction Eq. (1.10). This Airy type spectrum is observed most easily near the band edges.

When two-dimensional systems are considered, another complexity arises due to the freedom of the direction of the electric field with respect to the symmetry axis of the lattice. Except for the trivial case of [1 0], the periodicity along the field direction is an irregular function of the angle between the field and the [1 0] direction. In the irrational direction, where the tangent of the angle is irrational,

the periodicity length can not be defined. It is not trivial to answer the question whether or not the physically observable quantity such as the density of states is a smooth function of the angle. It is also interesting to see how the edge states are modified in two–dimensions.

In this chapter, to answer the above questions, we investigate the energy spectra in the two–dimensional tight–binding model of the square lattice when the electric field is applied in various directions. The model system may be realizable in the quantum dot lattices made of semiconductors, in which the lattice spacing is controllable, and the strong field condition considered in this chapter may be fulfilled easily by experimentally accessible field strengths.

The organization of this chapter is the following. In the following Section, we calculate the energy spectra analytically assuming the periodic boundary conditions. In Section 2.3, the model for the numerical calculation is given. The energy spectra, the density of states and the wave functions are studied by numerical calculations for systems of finite size in Section 2.4. Section 2.5 is devoted to discussion and the summary is given in the final section.

2.2 Solutions for Bulk States

We consider electrons on a two–dimensional lattice described by the tight–binding model. The Hamiltonian is given by

$$H = -t \sum_{x,y} \sum_{(\alpha,\beta)=(\pm 1,0),(0,\pm 1)} a^{\dagger}_{x+\alpha,y+\beta} a_{x,y} + \sum_{x,y} \frac{F}{\sqrt{M^2+N^2}} (Mx+Ny)\, a^{\dagger}_{x,y} a_{x,y}, \quad (2.1)$$

where $a^{\dagger}_{x,y}(a_{x,y})$ creates (annihilates) an electron at site (x, y), t the transfer integral between the nearest neighbor sites and the lattice constant a is set unity. The electric field is assumed to be applied along the direction $[M,\ N]$ with M and N being relatively prime integers.

When the electric field is applied in the direction of the crystal axis, *i.e.*, $[M, N] =$ [1 0], the Hamiltonian (2.1) is easily diagonalized and the eigenvalues are explicitly written as

$$E(\nu, k) = F\nu - 2t\cos k, \quad (k = 2\pi n/L; \quad \nu = 0, \cdots, L-1), \quad (2.2)$$

and the corresponding wavefunction is given by

$$C_{\nu,k}(x, y) = L^{-1/2} J_{x-\nu}(2t/F) \mathrm{e}^{iky}, \quad (2.3)$$

where ν is an integer. In the above L is the system linear dimension and the periodic boundary condition is assumed. The first term originates from the Stark ladder states along the x–direction where ν corresponds to the gravity center of the squared eigenfunction, and the second comes from the hopping of electrons in the y–direction. In this case, the energy spectrum consists of multiple bands, the centers of which are located in a equi–distant manner.

When the field is not in the direction of the crystal axis, *i.e.*, $[M, N] \neq$ [1 0], the Schrödinger equation for the Hamiltonian (2.1) is not decoupled into the equations

for the x– and y–directions. To obtain the energy spectrum in this case, we rotate the coordinate (x, y) to (ξ, η) by

$$\begin{aligned} \xi &= (Mx + Ny)/\sqrt{M^2 + N^2}, \\ \eta &= (-Nx + My)/\sqrt{M^2 + N^2}, \end{aligned} \tag{2.4}$$

where the direction of the axis ξ is parallel to the electric field and that of η perpendicular to it. Then by the standard argument in crystallography, the equivalent lattice net lines $\{M, N\}$ are characterized by the integral values of $\xi\sqrt{M^2 + N^2}$, and the distance between the nearest neighbor net lines is given by $d = 1/\sqrt{M^2 + N^2}$. On each of the net lines the lattice points are located $1/d$ apart. The eigenfunction ψ is given by the linear combination of the wave function at each site,

$$\psi = \sum_{\xi,\eta} C(\xi, \eta)|\xi, \eta\rangle, \tag{2.5}$$

where $|\xi, \eta\rangle$ is the state localized at site (ξ, η) and $C(\xi, \eta)$ is its amplitude. From equations (2.1) and (2.5), we obtain

$$\begin{aligned} &-t\{C(\xi + Nd, \eta + Md) + C(\xi - Nd, \eta - Md) + C(\xi + Md, \eta - Nd) \\ &+C(\xi - Md, \eta + Nd)\} \quad + F\xi C(\xi, \eta) = EC(\xi, \eta). \end{aligned} \tag{2.6}$$

We assume the periodic boundary condition along the η–direction with the period $L = K/d$ where K is a positive integer, viz.,

$$C(\xi, \eta + L) = C(\xi, \eta), \tag{2.7}$$

and Fourier transform $C(\xi, \eta)$ by

$$C(\xi, \eta) = \frac{1}{L} \sum_{m=0}^{Ld-1} \mathrm{e}^{iq\eta} C_q(\xi), \tag{2.8}$$

where

$$q = 2\pi m/L - \pi d, \quad (m = 0, 1, \cdots, Ld - 1). \tag{2.9}$$

Then we have

$$-t\left\{e^{iMdq}C_q(\xi+Nd)+e^{-iMdq}C_q(\xi-Nd)\right.$$
$$\left.+e^{-iNdq}C_q(\xi+Md)+e^{iNdq}C_q(\xi-Md)\right\}+F\xi C_q(\xi)=EC_q(\xi). \quad (2.10)$$

Next, the periodic boundary condition along the ξ–direction is imposed, viz.,

$$C_q(\xi+L)=C_q(\xi), \quad (2.11)$$

and the amplitude is Fourier transformed by

$$C_q(\xi)=\frac{1}{L}\sum_{l=0}^{L/d-1}e^{ip\xi}C_{p,q}, \quad (2.12)$$

where

$$p=2\pi l/L-\pi/d, \quad (l=0,1,\cdots,L/d-1). \quad (2.13)$$

Then we have

$$C_{p+2\pi/d,q}=C_{p,q}. \quad (2.14)$$

The ξ–linear term in Eq.(2.10) can be transformed to

$$\begin{aligned}\xi\ C_q(\xi) &= \frac{1}{2\pi}\int_0^{2\pi/d}dp\ \ \xi e^{ip\xi}C_{p,q}\\ &= \frac{1}{2\pi}\int_0^{2\pi/d}dp\ \ e^{ip\xi}i\frac{\partial}{\partial p}C_{p,q}, \end{aligned} \quad (2.15)$$

where the integral by parts was performed to reach the final line. We obtain from (2.10),

$$\frac{\partial C_{p,q}}{\partial p}=-i\frac{E-\epsilon(p,q)}{F}C_{p,q}, \quad (2.16)$$

where,

$$\epsilon(p,q)=-2t\left\{\cos d(Mp-Nq)+\cos d(Np+Mq)\right\}, \quad (2.17)$$

and the solution of (2.16) is given by

$$C_{p,q}\propto\exp\left[-\frac{i}{F}\int_0^p\left\{E-\epsilon(p',q)\right\}dp'\right]. \quad (2.18)$$

The periodicity condition (2.14) leads to

$$E = Fd\nu, \quad (\nu = \text{integer}). \tag{2.19}$$

This result indicates that there is no dispersion in E like (2.2) and to each Stark ladder state there correspond Ld different values of the wavenumber q, or in other words, the degeneracy factor is K. This is because in the case of general $[M, N]$, the hopping of the electron onto the sites on the same equi-potential line, *i.e.*, on the same net line, is forbidden while it is allowed for [1 0] case.

The wavefunction $C_q(\xi)$ as obtained by the inverse Fourier transformation of (2.18) is localized within the length of the order of λ given by (1.8). For example, in the case of $[M, N] = [1\ 1]$ the wave function (2.17) is rewritten as

$$C_q(\xi) = \begin{cases} J_{\sqrt{2}\xi-\nu}\left(4\sqrt{2}t\cos\left(q/\sqrt{2}\right)/F\right), & \text{for } \cos q/\sqrt{2} \neq 0, \\ \delta_{\sqrt{2}\xi-\nu,0}\ , & \text{for } \cos q/\sqrt{2} = 0, \end{cases} \tag{2.20}$$

and the localization length is given by $4\sqrt{2}t\cos\left(q/\sqrt{2}\right)/F$ which is q-dependent.

The treatment here is valid as long as the localization length is much smaller than the system size, and in a finite system the energy spectrum (2.19) is realized only in the band center when $W_0/F \lesssim L$, or $V \gtrsim W_0$ where $V = FL$ is the potential drop through the system and $W_0 = 8t$ the bandwidth for the zero field. However effects of the boundaries have not been considered in the above derivation. Since the states near the system edges are difficult to discuss quantitatively by the analytic calculation, we will perform numerical calculations of Eq. (2.10) in the next section.

2.3 Model for the Numerical Calculation

The super cell used in our numerical calculation is illustrated in Fig. 2.1, and the lattice is assumed to be composed of $K \times K$ super cells where K is a positive integer, or in other words the system linear dimension is given by $L = K\sqrt{M^2 + N^2}$. Integer K is so chosen that L remains roughly constant (≈ 150) for various directions of the electric fields. Typically $K = 6 \sim 20$ in our calculations.

The density of states per site is defined by

$$\begin{aligned} D(E) &= \frac{1}{L^2}\sum_i \delta(E - E_i) \\ &= \lim_{\Delta \to +0} \sum_i \frac{1}{L^2\sqrt{\pi}\Delta} \exp\left\{-(E - E_i)^2/\Delta^2\right\}, \end{aligned} \tag{2.21}$$

where E_i is the i–th eigenvalue. To avoid the divergence due to the delta function, we set Δ to be a finite value in (2.21), instead of taking the limit to zero. We take $\Delta = (W_0 + V)/2L$, which means that Δ is comparable to each ladder separation in the Stark ladder region. The energy origin is taken to be $E = V/2$.

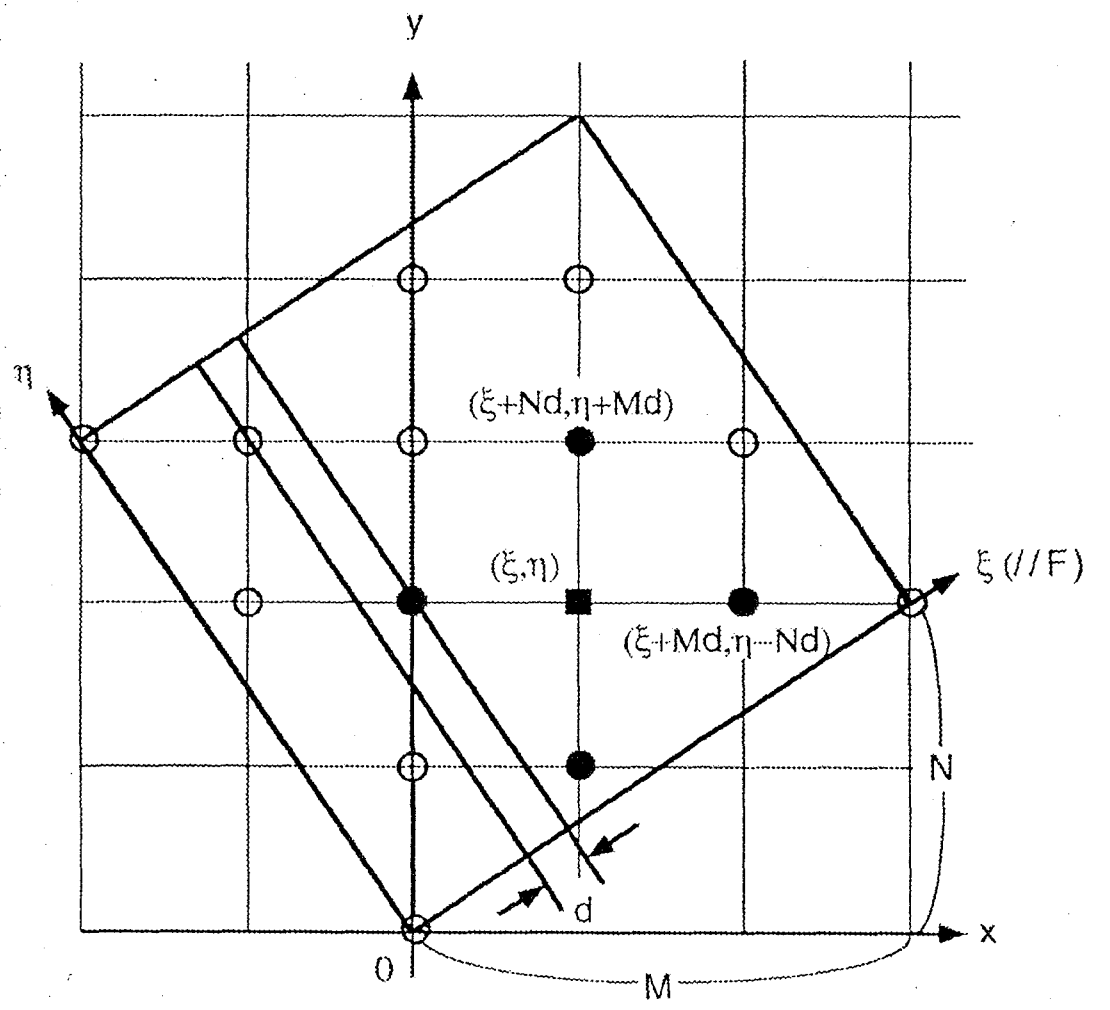

Figure 2.1: Slanted super cell for the electric field direction $[M, N]$. The electron at site $[\xi, \eta]$ can hop to $[\xi + Md, \eta - Nd]$, $[\xi + Nd, \eta + Md]$, $[\xi - Md, \eta + Nd]$ and $[\xi - Nd, \eta - Md]$, where $d = (M^2 + N^2)^{-1/2}$ is the separation between the nearest net lines.

2.4 Numerical Results in Finite Systems

The eigenvalues, density of states and wavefunctions in two–dimensional tight–binding model in the electric field are numerically studied based on Eq. (2.1) with the periodic boundary conditions when the direction and magnitude are changed.. The density of states is calculated for weak ($V = 0.5W_0$), intermediate ($V = W_0$) and strong ($V = 16W_0$) electric fields. In Fig. 2.2a, the density of states in the weak electric field is shown for the case of the nonsymmetric direction $[M, N] = [3\ 1]$. The logarithmic singularity, *i.e.*, the van Hove singularity of the density of states[†] of the 2D square lattice at the center , which exists at $F = 0$, disappears. Near the band edges there appear oscillations of the density of states, and the energy position of the i–th peak counted from the band bottom is written by $|Z_i|\,(t\ F^2)^{1/3} + \text{const.}$ as given by Eq. (1.11). Thus the eigenenergies are understood as the sum of $|Z_i|\,(t\ F^2)^{1/3}$ and a term originating from the degree of freedom perpendicular to the field. This point will be discussed in Section 2.5. The bandwidth is of the order of $W_0 + V$. We have confirmed that the density of states is almost independent of the direction of the electric field in these magnitudes of the field strength as shown below.

In the intermediate electric field shown in Fig. 2.2b, the Stark ladder states do not appear, because the wavefunctions still extend through the system. We have

[†]The density of states in two dimensional square lattice is given by

$$D(E) = \frac{1}{L^2}\sum_{\mathrm{k}} \delta(E - E_{\mathrm{k}}) = \frac{1}{2t\pi^2} K\left(\sqrt{1 - \left(\frac{E}{4t}\right)^2}\right),$$

where $K(k) = \int_0^{\pi/2} d\theta (1 - k^2 \sin^2\theta)^{-1/2}$ is the elliptic integral. Thus, the density of states near the band center ($|E| \approx 0$) is approximately given by

$$D(E) \approx \frac{1}{2t\pi^2}\left\{\frac{1}{2}\ln\left(\left(\frac{8t}{E}\right)^2 - 1\right) + 1\right\}.$$

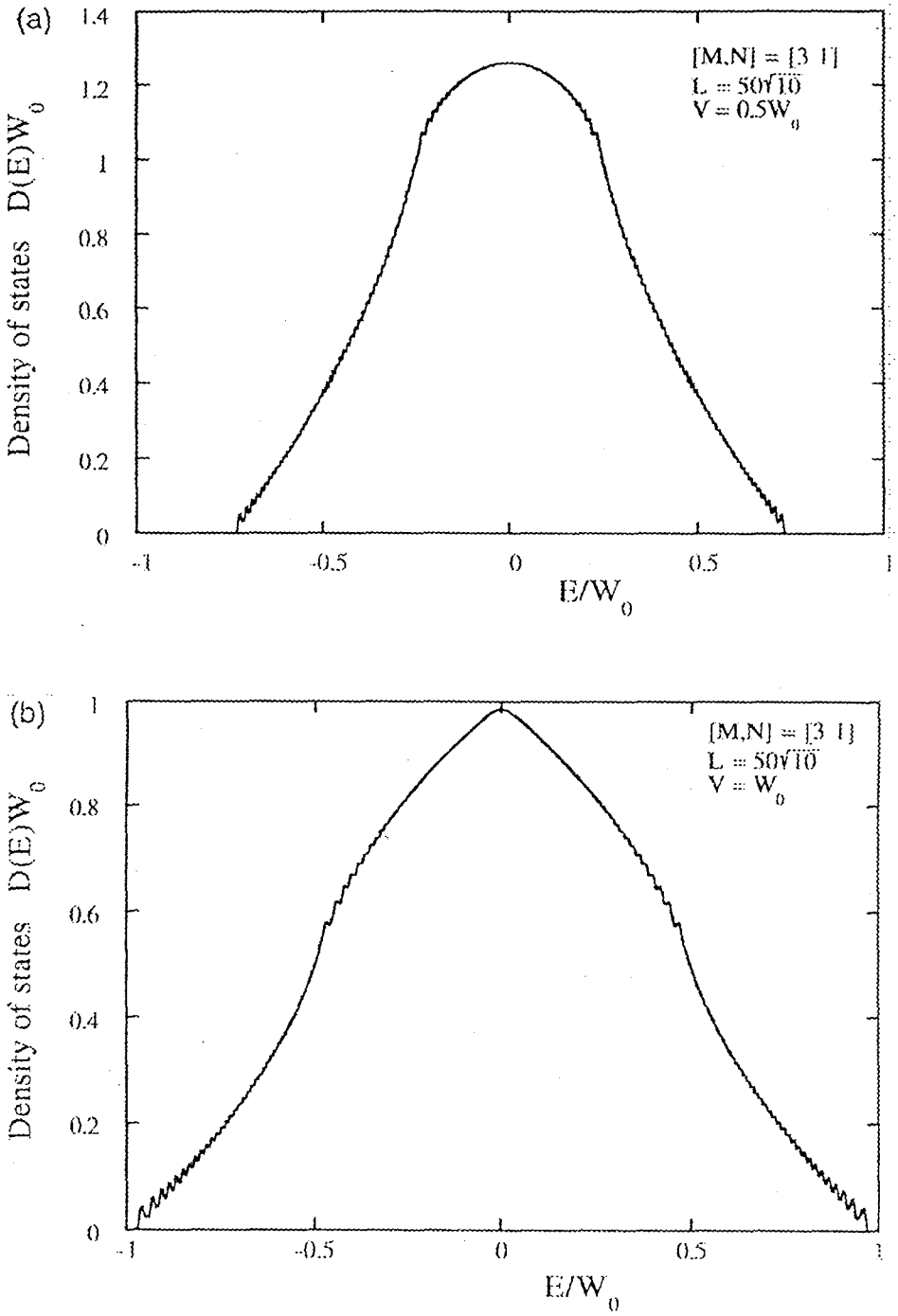

Figure 2.2: Electric field dependence of the density of states for the field direction $[M, N] = [3\ 1]$ at (a) the weak electric field $V = 0.5W_0$ and at (b) the intermediate electric field $V = W_0$, where $W_0 = 8t$ is the bandwidth at zero electric field, V the potential drop across the lattice, and L the lattice linear dimension.

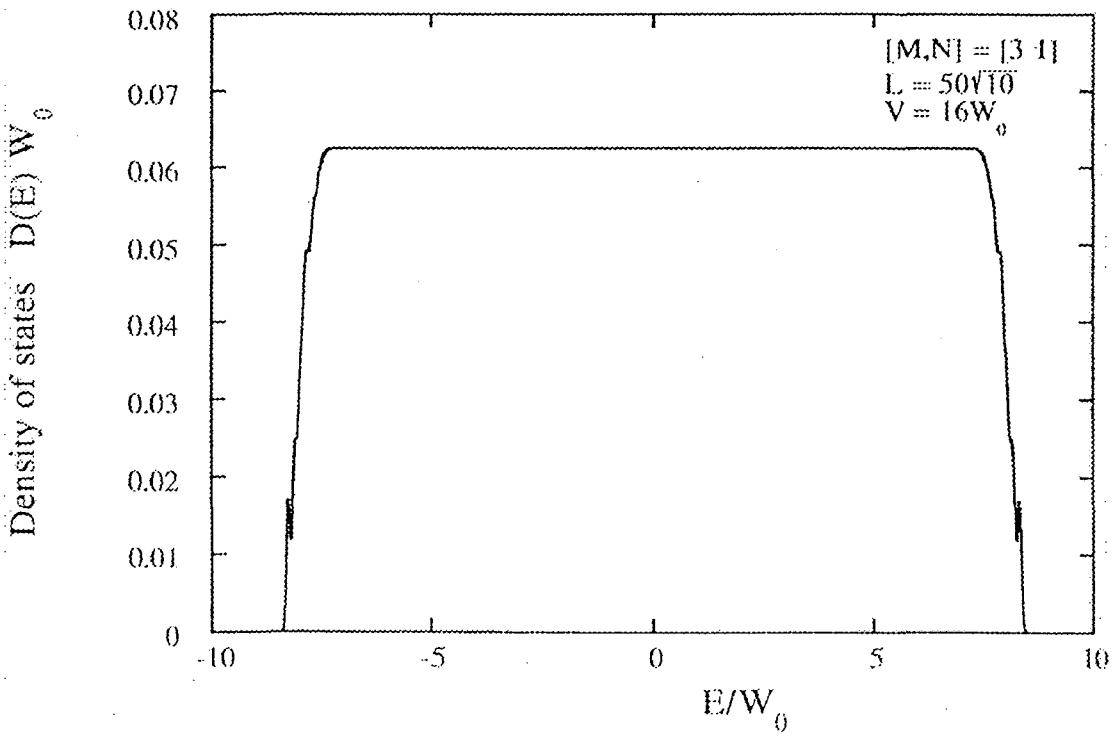

Figure 2.3: Density of states at the strong electric field $V = 16W_0$ for the direction $[M, N] = [3\ 1]$.

confirmed that the Stark ladder states appear in the band center, when the electric field is greater than W_0/L. This is consistent with the argument in Section 2.2 that wavefunctions for the Stark ladder states are localized along the field direction within the length of the order of $\lambda \approx W_0/2F$.

In Fig. 2.3, an example of the density of states is plotted for the strong electric field ($V = 16W_0$). It is flat near the band center indicating the existence of the Stark ladder. The density of states in the flat region is $1/V$, which is confirmed to be independent of the direction of the electric field. This indicates that the energy spacing is $F/\sqrt{M^2 + N^2}$ and the degeneracy factor of each level in the band center is $L/\sqrt{M^2 + N^2} = K$ as discussed for the infinite lattice in Section 2.2 and the factor $\sqrt{M^2 + N^2}$ cancels out in the density of states. These discretized eigenvalues for

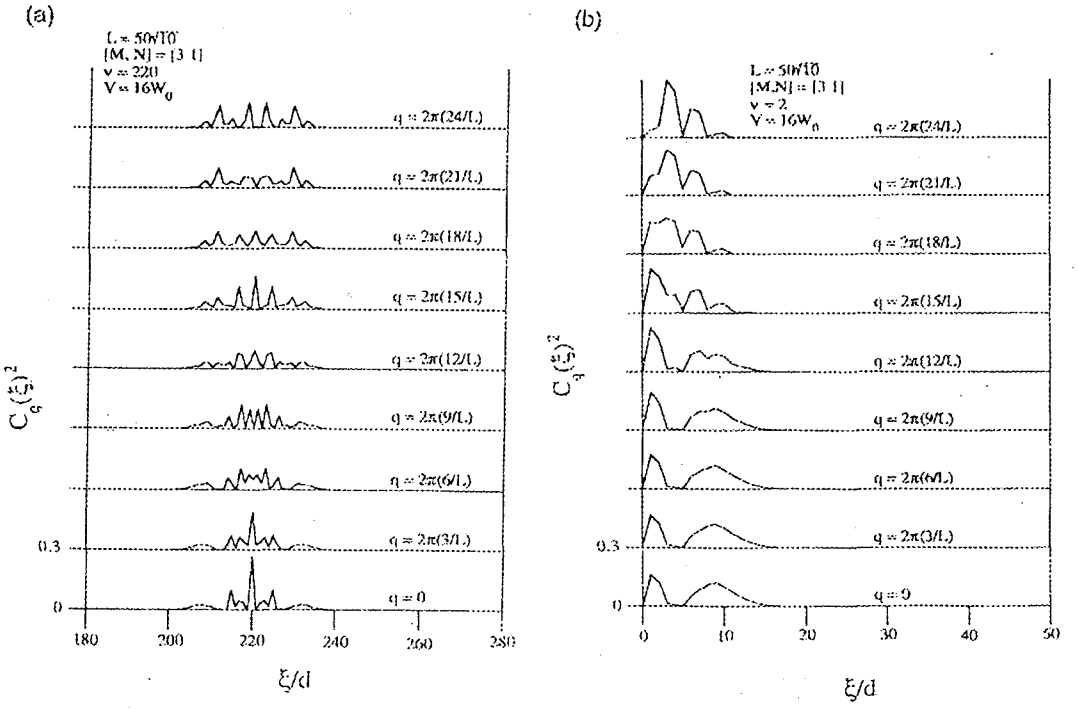

Figure 2.4: The squared amplitude of wavefunctions for the eigenvalues (a) $\nu = 220$ and (b)$\nu = 2$, where $d = (M^2 + N^2)^{-1/2}$ is the equivalent net line distance.

the nonsymmetric direction are contrasted to the continuous eigenvalues of (2.2) for the symmetric direction. When the electric field is applied parallel to the symmetry direction, *i.e.*, $[M, N] = [1\ 0]$, the density of states is given by the superposition of 1D density of states centered at $E = F\nu$, and is not flat but has oscillations which is clearly seen due to the 1D van Hove singularity. Near the band edges, oscillatory peaks are seen in Fig. 2.3, which are again due to the Airy type spectrum as in the weak electric field case.

In Fig. 2.4a, we show an example of the squared amplitude of the wavefunction $C_q(\xi)$ corresponding to a state near the band center for $V = 16W_0$ and $[M, N] = [3\ 1]$. It is seen that they are symmetric and that the characteristic localization length is of the order of W_0/F similar to the 1D case. In Fig. 2.4b, we show the squared

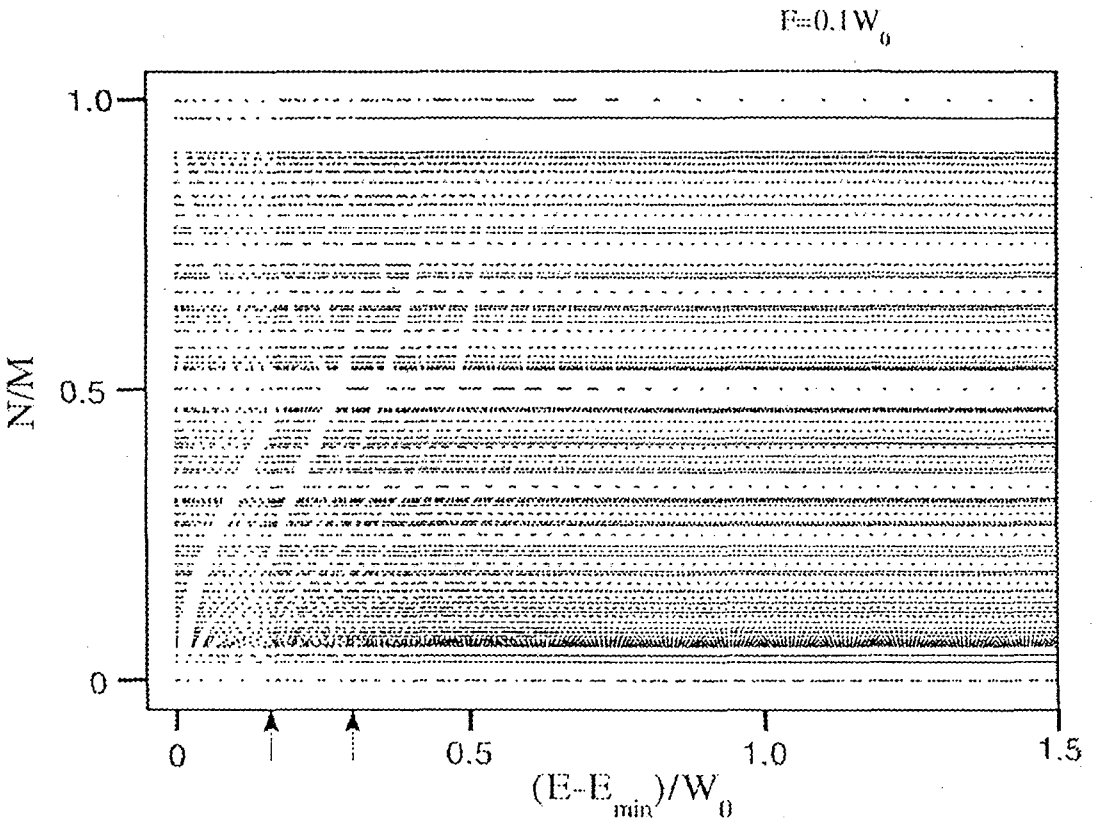

Figure 2.5: The direction of the electric field N/M vs. the eigenenergies in the lower band region for $F = 0.1W_0$. Arrows indicate the dense energy positions.

wavefunction amplitude corresponding to the state near the band edge. As discussed before, the behavior of the wavefunction parallel to the electric field is characterized essentially by the Airy function.

To see these edge levels in detail, the energy spectrum is plotted in Fig. 2.5 for different electric field directions. The magnitude of the electric field $F = 0.1W_0$ is fixed which is nearly equivalent to the strong field case $V = 16W_0$. Near the band edge, there are regions where the states become more dense than the lower energy region of which are independent of the field direction (see arrows in the figure). These dense regions correspond to the Airy type spectrum and show up as peaks in the

density of states in Fig. 2.3.

It is remarkable that many energy gaps which are not related to the Airy states are seen in the lower energy region and their magnitude and location vary continuously with the field direction N/M. It is confirmed that these gaps do not appreciably depend on the lattice size L for constant F. These gaps are not clearly seen in the density of states in Fig. 2.3, because the width Δ in (2.21) is taken to be larger than these gaps. The physical origin of these energy gaps is discussed in next section.

2.5 Discussion about Edge States

First we discuss the Airy states in the two dimensional lattice. To obtain wavefunctions and eigenenergies for the edge states for the general direction $[M, N]$, we expand the wavefunction in (2.10) around ξ up to the second order. The resulting second order differential equation with respect to ξ is easily converted to the Airy type equation. Assuming that the wavefunction vanishes at the boundary $\xi = 0$, we obtain, apart from the normalization factor,

$$C_q^i(\xi) = \exp\{-iB(q)\xi/2D(q)\}\mathrm{Ai}\left(\left(\frac{F}{D(q)}\right)^{1/3}\xi + Z_i\right), \tag{2.22}$$

with the corresponding eigenenergy

$$E_i(q) = |Z_i|(F^2 D(q))^{1/3} - \frac{B(q)^2 + 4A(q)D(q)}{4D(q)}, \tag{2.23}$$

where

$$\begin{aligned} A(q) &= 2t(\cos Mdq + \cos Ndq), \\ B(q) &= 2td(N\sin Mdq - M\sin Ndq), \\ D(q) &= td^2(N^2\cos Mdq + M^2\cos Ndq). \end{aligned} \tag{2.24}$$

This is an obvious extension of the one dimensional version given in (1.10). The first term represents the Airy steps and the second the dispersion. Since $|q|$ is smaller than πd as seen from (2.9), we obtain

$$E_i(q) \approx |Z_i|\left\{F^2t(1 - M^2N^2d^4q^2)\right\}^{1/3} - 4t(1 - q^2/4) + o(q^2), \tag{2.25}$$

for small q. This indicates that the energy is quantized to $|Z_i|(F^2t)^{1/3}$ with the width of the order of $|Z_i|(F^2t)^{1/3}(MNd^2)^2q^2/3$. We understand that the dense region in Fig. 2.5 which is independent of the direction of the electric field corresponds to the

Airy steps. The oscillation of the density of states as seen in Figs. 2.2 and 2.3 is also explained by this eigenenergy Eq. (2.25). The peak positions in Fig. 2.2a measured from the first peak are $1.85\times10^{-2}, 3.36\times10^{-2}, 4.69\times10^{-2}, \ldots$, and the corresponding values estimated from eigenenergies (2.25) are $1.88\times10^{-2}, 3.43\times10^{-2}, 4.79\times10^{-2}, \ldots$, and their correspondence is satisfactory.

Next, we consider the gaps shown in Fig. 2.5. To see the electric field dependence of the gaps, the energy spectrum is replotted as a function of the electric field in Fig. 2.6a, where the direction of the electric field is fixed to $[M, N] = [6\ 1]$. At sufficiently high electric field, the energy spectrum is quantized to the Stark ladder levels. As the electric field decreases, the Stark levels are broadened and the energy spacings among them become narrowed, and finally the energy levels become continuous at sufficiently small electric field. In Fig. 2.6b, the similar plot is shown for $[M, N] = [11\ 2]$ which is close to the direction $[M, N] = [6\ 1]$. The magnitude of gaps decreases with decreasing field similarly to the case of $[M, N] = [6\ 1]$. It is remarkable that the magnitude and location of the second gap for $[M, N] = [11\ 2]$ is nearly equal to the first gap for $[M, N] = [6\ 1]$. In the case of general direction $[M, N]$, it is confirmed that the Nn–th energy gap counted from the bottom, with n an integer, persists until the field becomes small enough $F = 0.1W_0$ and that other gaps are destroyed at rather high fields. The magnitudes and the locations of the persisting gaps are continuous functions of the field direction N/M. The gaps seen in Fig. 2.5 correspond to the above mentioned persisting gaps. These phenomena are understood qualitatively as follows. In the general direction of $[M, N]$, first N net lines from the system edge have no hopping lattice points at the edge side (cf. Fig. 2.1). As a general rule, the environment of the n–th group of net lines located at $Nn + 1, Nn + 2, \ldots, Nn + N$ from the edge is similar. The eigenenergy $E_i(q)$ of

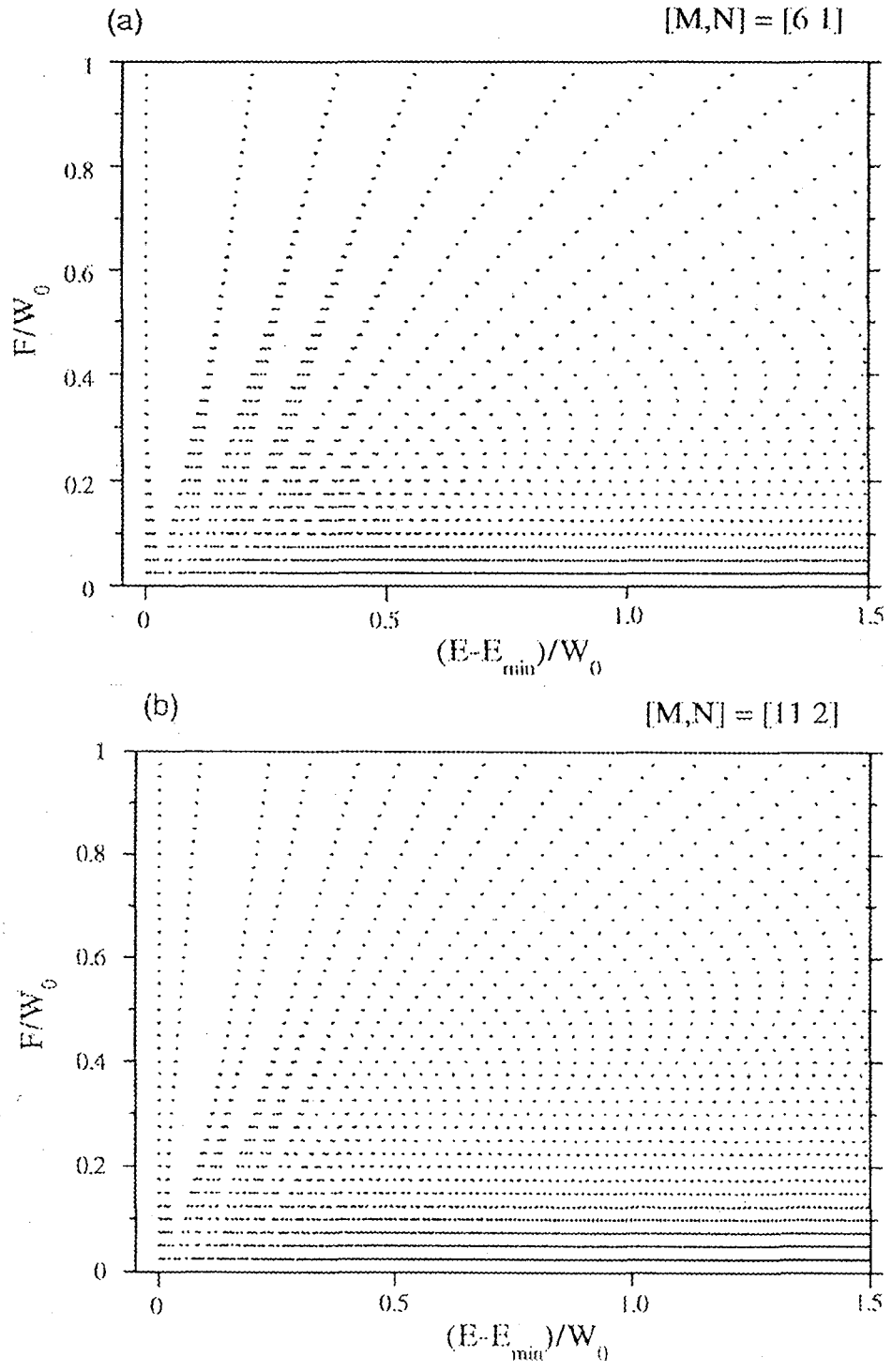

Figure 2.6: The electric field dependence of the eigenenergies for fixed field directions, (a) $[M, N] = [6\ 1]$ and (b) $[M, N] = [11\ 2]$.

the edge state is closely related to the position of the wavefunction since the gravity center of the wavefunction $\langle \xi \rangle_{iq}$ is given by $\partial E_i(q)/\partial F$ by Feynman–Hellman theorem [55]. Therefore, the above situation leads to the result that each group of N eigenenergies is almost degenerate and gaps open between each groups. The mean positions of the gaps are also controlled by $\langle \xi \rangle$, which will be a smooth function of the angle.

Finally we discuss the characteristic parameters of our calculations. The overall shape of the density of states, such as the bandwidth or the region of energy where the Stark ladder states exist, is characterized by the potential drop $V = FL$. On the other hand the edge states are governed by the field strength F, e.g., separation of the oscillations in the density of states near the band edges. There are no direct system size dependence within the sizes performed in our calculations as long as they are scaled properly by V or F. It should be noted also that the choice of the boundary conditions, either periodic or Dirichlet type, does not alter the conclusions given above.

2.6 Summary of Chapter 2

In this chapter, the electronic states of a two–dimensional tight–binding model in a uniform electric field are studied in which the direction of electric field is varied. It is shown that the magnitude of the density of states at the plateau on the center of the band region is independent of the field direction when the Stark ladder states appear, although the periodicity of the crystal along the electric field is a chaotic function of the field direction, and hence the Stark ladder spacing becomes erratic. By looking at the finite lattice, we find that the edge states are characterized by the Airy spectrum and that some unexpected energy gaps appear for the appropriate electric field strength. The features found in the finite lattice, if they are properly scaled by either F or V, do not depend explicitly on the system size.

Chapter 3

Two–Dimensional Tight–Binding Lattice in Electric and Magnetic Fields

Electronic states of a two–dimensional tight–binding model on a two–dimensional square lattice with finite size in the presence of both uniform electric and magnetic fields are studied. Numerical solutions for eigenenergies are presented. The magnetic subbands at zero electric field known as the Hofstadter butterfly are modified by the electric field and the eigenenergies for high electric fields are represented by the Stark ladder states associated with each of the magnetic subbands. When the electric potential drop across the system becomes comparable to the bandwidth of zero field, the density of states becomes the pyramid shape with steps, the steps being induced by the finiteness of the lattice. The influence on the density of states by the change of the direction of the electric field is also discussed.

3.1 Introduction to Chapter 3

It is known that the electronic spectrum of a two–dimensional tight–binding model in high magnetic fields shows a fairly complicated structure [33–35]. The structure often called the Hofstadter butterfly is characterized by the self–similarity and by multiple magnetic subbands with gaps induced by the magnetic field [33,36]. When the magnetic flux ϕ per unit cell is equal to $(p/q)\phi_0$, where p and q are mutually prime integers and $\phi_0 = ch/e$ is the flux quantum, the spectrum is divided into q magnetic subbands with gaps in between. This model is studied in several papers [37–40] as a trial towards the understanding of the quantized Hall effect [41].

When a magnetic field is switched off and only an electric field $\mathcal{E}$ is applied parallel to the lattice as discussed in Chapter 2, the wavefunctions are localized in parallel to the electric field and a set of discrete eigenenergies called Stark ladders is generated for sufficiently strong electric fields [1,2,6,10,11]. Its energy level spacing is uniform and is equal to the potential drop across the lattice periodicity length. When the electric field is applied parallel to the direction $[M, N]$, where M and N are integers prime to each other, the periodicity length d in units of the lattice constant a is given by $d = (M^2 + N^2)^{-1/2}$ and the ladder spacing is given by Fd where $F = e\mathcal{E}a$ with $-e$ the electron charge [56,57]. When the angle θ ($\tan\theta = N/M$) between the electric field and the symmetry axis is changed slightly, a pair of M and N changes irregularly, so that the periodicity length becomes an erratic function of θ. In the irrational direction, where $\tan\theta$ is irrational, the periodicity length is no more well–defined. In this connection the question will be raised whether or not this irregularity is reflected in the observable quantities such as the density of states. The dependence of the energy spectrum on the angle between external electric field and crystal axis has been investigated in a previous chapter [56,57] when magnetic field is absent. It

has been shown that the smeared out density of states becomes independent of the direction of the electric field at strong fields, though the level separation Fd varies discontinuously with the change of the field direction.

When both the electric and magnetic fields are present [52,53], the question arises whether or not the gaps induced by the magnetic field remain stable and how the energy spectrum is modified. In this chapter we analyze the interplay of magnetic and electric fields to answer these questions. We investigate the energy spectra in the two-dimensional tight-binding model of the square lattice with the magnetic field applied normal to the surface and the electric field applied in various directions parallel to the surface. The organization of this chapter is the following. In Section 3.2 we introduce the Harper equation [46] modified by the electric field term. In Section 3.3, the energy spectra and the density of states are calculated numerically for lattices of finite size assuming the periodic boundary conditions. Section 3.4 is devoted to discussion on the symmetries of this model and the summary is given in the final section.

3.2 Two–Dimensional Tight–Binding Model on Crossed Electric and Magnetic Fields

We consider a tight–binding model with a nearest–neighbor transfer integral $-t$ on a square lattice with lattice constant a. We assume that an electric field $\mathcal{E}$ is applied parallel to the direction $[M, N]$, and a magnetic field B normal to the lattice plane. It is convenient to use the following gauge for the vector potential:

$$\mathbf{A} = \left(-\frac{N(Mx+Ny)}{M^2+N^2}, \frac{M(Mx+Ny)}{M^2+N^2} \right) B. \tag{3.1}$$

The effect of the magnetic field is taken into account by the Peierls phase factor [42] of the transfer integral, and the Hamiltonian is given by

$$\begin{aligned} H = \; & -t \sum_{x,y} \left[a^\dagger_{x+1,y} a_{x,y} e^{i2\pi\phi N(M(x+1/2)+Ny)d^2} \right. \\ & + \left. a^\dagger_{x,y+1} a_{x,y} e^{-i2\pi\phi M(Mx+N(y+1/2))d^2} + h.c. \right] \\ & + \sum_{x,y} Fd(Mx+Ny) a^\dagger_{x,y} a_{x,y}, \end{aligned} \tag{3.2}$$

where $a^\dagger_{x,y}(a_{x,y})$ creates (annihilates) an electron at site (x, y), $F = e\mathcal{E}a$ is the electric potential drop across the lattice constant a, $\phi = Ba^2$ the magnetic flux per unit cell and $d = a/\sqrt{M^2+N^2}$. In the above, units are chosen such that the lattice constant a and the magnetic flux quantum $\phi_0 = ch/e$ are unity.

For later convenience we rotate the coordinate system and define a new set of variables ξ and η by

$$\begin{cases} \xi = (Mx+Ny)/\sqrt{M^2+N^2}, \\ \eta = (-Nx+My)/\sqrt{M^2+N^2}, \end{cases} \tag{3.3}$$

where the direction of the axis ξ is parallel to the electric field and η perpendicular to it. Then by the standard argument in crystallography, the equivalent lattice net lines $\{M, N\}$ are characterized by the integral values of $\xi\sqrt{M^2+N^2}$, and the

distance between the nearest neighbor net lines is given by $d = 1/\sqrt{M^2 + N^2}$. On each of the net line the lattice points are located $1/d$ apart. These transformations lead to the Schrödinger equation:

$$\begin{aligned} -t\,[&C(\xi + Nd, \eta + Md) \exp\{-i2\pi\phi Md(\xi + Nd/2)\} \\ +\ &C(\xi - Nd, \eta - Md) \exp\{i2\pi\phi Md(\xi - Nd/2)\} \\ +\ &C(\xi + Md, \eta - Nd) \exp\{i2\pi\phi Nd(\xi + Md/2)\} \\ +\ &C(\xi - Md, \eta + Nd) \exp\{-i2\pi\phi Nd(\xi - Md/2)\}] \\ +\ &F\xi C(\xi, \eta) = E\ C(\xi, \eta), \end{aligned} \tag{3.4}$$

where $C(\xi, \eta)$ is the amplitude of the eigenfunction on site (ξ, η). We assume here the periodic boundary condition along the η direction with a period $L = K/d$ where L is the system size and K a positive integer, viz.,

$$C(\xi, \eta + L) = C(\xi, \eta), \tag{3.5}$$

and Fourier transform $C(\xi, \eta)$ by

$$C(\xi, \eta) = \frac{1}{L} \sum_{m=0}^{K-1} \mathrm{e}^{ik\eta} C_k(\xi), \tag{3.6}$$

where

$$k = 2\pi m/L - \pi d, \quad (m = 0, 1, \cdots, K-1). \tag{3.7}$$

Then we have

$$\begin{aligned} -t\Big\{&\mathrm{e}^{iMd(k-2\pi\phi(\xi+dN/2))} C_k(\xi + Nd) + \mathrm{e}^{-iMd(k-2\pi\phi(\xi-dN/2))} C_k(\xi - Nd) \\ +&\mathrm{e}^{-iNd(k-2\pi\phi(\xi+dM/2))} C_k(\xi + Md) + \mathrm{e}^{iNd(k-2\pi\phi(\xi-dM/2))} C_k(\xi - Md)\Big\} \\ &+F\xi C_k(\xi) \ = \ EC_k(\xi). \end{aligned} \tag{3.8}$$

The advantage of employing the gauge (3.1) is now clear. Namely, we can reduce the Hamiltonian for two dimensions into an equation for one dimension which contains the wavenumber k as a parameter, and the numerical treatment to derive the

eigenenergies becomes much easier than to analyze the original Hamiltonian (3.2). In the next section, the above Schrödinger equation is numerically solved with the boundary condition $C_k(\xi) = C_k(\xi + L)$ in various electric and magnetic fields, and the results will be shown.

3.3 Results of the Numerical Calculation

3.3.1 Density of States

In this section, the eigenvalues and the density of states of the two–dimensional tight–binding model given by (3.8) in the presence of both the electric and magnetic fields are numerically calculated under the periodic boundary conditions. Since in finite systems, the density of states consists of a set of delta functions, it is inconvenient for the graphical representation. We present here instead the smoothed density of states, which is the convolution with the Gaussian shape (Eq. (2.21)) with the appropriate width in the same manner in the Section 2.3 [56].

We first discuss the case where the direction of the electric field is parallel to the symmetry axis, *i.e.*, $[M, N] = [1\ 0]$. The density of states for various electric fields is shown in Fig. 3.1 with the lattice linear dimension $L = 400$. The magnetic flux is fixed to be $\phi = 1/4$ $(p = 1, q = 4)$. In the zero electric field, as shown in Fig. 3.1a, the density of states is known [58] to be symmetric with respect to E and be composed of q magnetic subbands, where central two subbands touch together at $E = 0$. For $\phi = 1/4$ the bandwidths of the 1st and 2nd magnetic subbands from the bottom are $\left(2\sqrt{2} - \sqrt{4 + 2\sqrt{2}}\right) W_0/8 = 0.0269W_0$ and $\sqrt{4 - 2\sqrt{2}}W_0/8 = 0.1353W_0$, respectively, the band–gap between them being $\left(\sqrt{4 + 2\sqrt{2}} - \sqrt{4 - 2\sqrt{2}}\right) W_0/8 = 0.1913W_0$, and the overall bandwidth of the four subbands is $W_0/\sqrt{2}$, where $W_0 = 8t$ is the bandwidth of the zero electric and magnetic fields [59,60].

For the non–zero electric field, the important parameter is the ratio V/W_0 where $V = FL$ is the potential drop through the system [11], since the Stark ladder states are expected to be generated when V becomes comparable to or greater than the magnetic subband widths. For small V, the bandwidth of each magnetic subband increases with V and the two subbands in the center merge into one to result in a

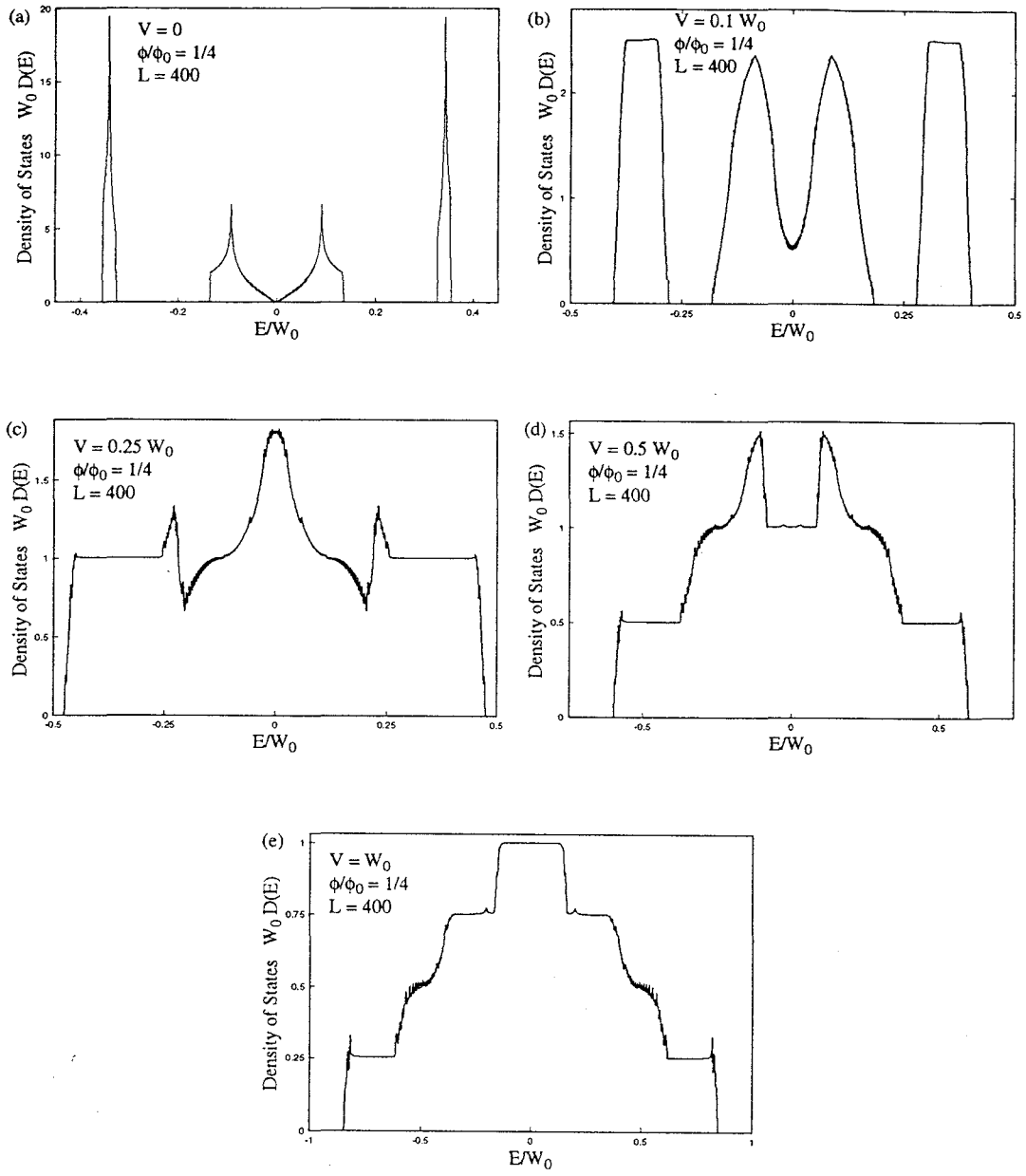

Figure 3.1: Electric field dependence of the density of states for the field direction $[M, N] = [1\ 0]$ and the magnetic flux $\phi/\phi_0 = 1/4$. The potential drop through the sample $V = FL$ is given by (a) $V/W_0 = 0$, (b) $V/W_0 = 0.1$, (c) $V/W_0 = 0.25$, (d) $V/W_0 = 0.5$ and (e) $V/W_0 = 1.0$, respectively, where L the sample length along the electric field and W_0 the bandwidth for zero magnetic and electric fields.

central subbands with two peaks and two subbands at both side as shown in Fig. 3.1b. The two subbands at both side has plateau in the center, which indicates that states in the subbands are in the Stark ladder states. The potential drop V is larger than the original subbandwidth of the both sided bands. As V is further increased, the two peaks in the middle merge into one, and the density of states gradually loses the original four peaked character to result in the three peaked shape as shown in Fig. 3.1c. In this figure, V equals $0.25W_0$ which is equal to the energy distance between the two peaks of the first and the second magnetic subbands at $V = 0$. For this value of V, the widths of the two central magnetic subbands are widened and the overlap of these two bands at $E \simeq 0$ becomes appreciable so that two subbands merge into one to form a single peak at the center. There are two peaks on either side. The peak consists from the overlap of the outer and inner subband. With increasing V, two peaks on both sides in Fig. 3.1c grow to reach the stage where the central peak is no more observable and only the two pronounced peaks are seen on the two-stepped mesa as shown in Fig. 3.1d. The reason why the shape of the density of states becomes the stepped mesa is understood qualitatively in the following way. When only the magnetic field is applied with the flux $\phi = p/q$ per unit area, the band is split into q magnetic subbands as mentioned before. When the parallel electric field is introduced in addition to the magnetic field, q sets of the Stark ladder states will be formed which are associated with each of the magnetic subbands [22,24,27,28]. The step-height of the mesa is roughly given by $W_0/(4V)$, since the density of states is given by $1/(qFL)$ as will be explained in the next section. Thus the step-height of the density of states indicates the number of the overlapped Stark ladders which originate from each of the magnetic subbands. The two peaks seen in the density of states in Fig. 3.1d are caused by the small overlap of three sets of the Stark ladders.

In the strong field such that V becomes of the order of W_0, the density of states becomes the pyramid shape with q steps as shown in Fig. 3.1e. The first, third and fourth steps are almost flat, indicating that the Stark ladders are formed for all of the four subbands. At the second step, the density of states has wiggles unlike other steps. These are caused by the edge states where the wavefunctions are localized near the sample edge ($X \approx \pm L/2$) because of the triangular potential at both ends and their eigenvalues are not equi-distant. Note also that the total bandwidth increases monotonically with the electric field, and is roughly given by $V + W_0$ for the strong enough field $V \gtrsim W_0$. In the extreme electric field such that $F \gtrsim W_0$ or $V \gtrsim W_0 L$, where L is the system size normalized by the lattice constant a, the density of states becomes structureless showing only one flat plateau, the height of which is given by $1/F$.

In order to see the existence of the Stark ladder states more clearly, the eigenenergy against the gravity center of the eigenstate is plotted in Fig. 3.2 for $V = W_0$, where the gravity center X is defined by

$$X = \sum_{\xi} \xi |C_k(\xi)|^2. \tag{3.9}$$

The eigenenergies for $V = W_0$ are characterized by three bands with the same slope F (cf. also Fig. 3.1e). The constant slope indicates the formation of the Stark ladder states. The central wide band consists of the two dark narrow belts connected by a light wide belt in between. The two narrow belts in the middle and two detached bands located at the top and the bottom originates from the four magnetic subbands in the absence of F. The light wide belt in the center originates from the hybridized states of the two central magnetic subbands, where the wavefunctions are characterized by the resonating states between the two central subbands. The number of the hybridized states is smaller than the number of states

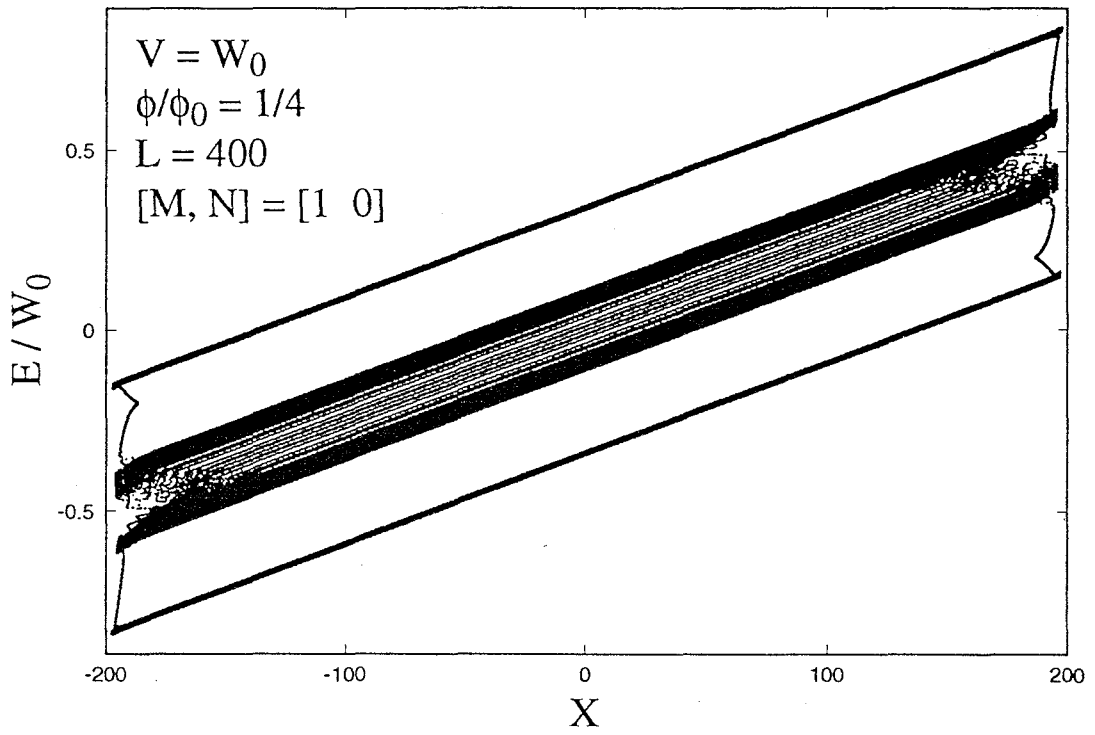

Figure 3.2: Eigenenergies against the gravity center X of the wavefunction for $V = W_0$ and $\phi/\phi_0 = 1/4$. Four sets of the Stark ladder states represented by dark belts are associated with each of the magnetic subbands.

on the bands which consist from two narrow belts in the middle and two detached bands located at the top and the bottom. Note that the edge states at both ends of the sample are clearly seen. The number of the edge states is much smaller than the bulk states, the ratio of which is of the order of L^{-1}. The number of overlapped bands is one for $|E/W_0| > 0.6$, two for $0.6 > |E/W_0| > 0.4$, three for $0.4 > |E/W_0| > 0.15$, and four for $|E/W_0| < 0.15$. These numbers are reflected into the steps in the density of states in Fig. 3.1e.

3.3.2 Magnetic Field Dependence of the Eigenenergy

In order to eliminate the shift of the energy by the electric field, $E - FX$ is plotted against the normalized magnetic flux for $V = W_0$ in Fig. 3.3. Here, in order to see

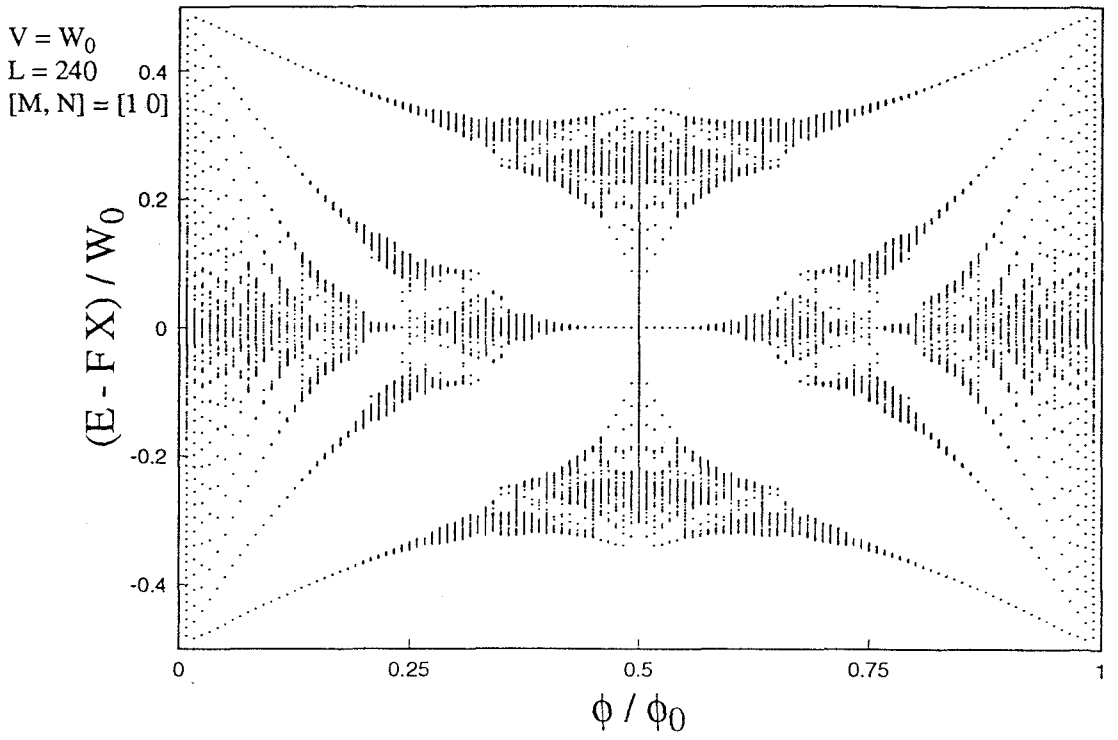

Figure 3.3: The magnetic field dependence of $E - FX$, where the energy states corresponding to the wave functions located at $|X| > L/4$ are omitted from the diagram.

the bulk property of the energy states, the wave functions located at $|X| > L/4$ are omitted from the diagram. The similarity of this diagram to the Hofstadter diagram shown in Fig. 1.1 [33] is clear, though some of the small band gaps are destroyed by the electric field. This similarity at moderate electric fields indicates that the eigenenergy E is given by the sum of the eigenenergy for zero electric field and the expectation value of the electric potential FX. When the localization length of the wavefunction is smaller than the magnetic length $l = \sqrt{\hbar/(eB)} = \sqrt{a^2\phi_0/(2\pi\phi)}$, the magnetic subbands merge into one. In the extreme electric field strength such that $F \approx W_0$ or $V \approx W_0 L$ all the gaps observed in Fig. 3.3 will be destroyed.

3.3.3 Dispersion Relation and the Dependence on the Direction of the Electric Field

In order to see the dependence on k for $[M, N] = [1\ 0]$, we plot $E - FX$ against k as shown in Fig. 3.4a. Most of the energy eigenvalues denoted by thick lines have the periodicity of $2\pi/q$ ($q = 4$ in this case). Thin lines with the k periodicity which are going parallel to the thick lines around $|E - FX| \simeq 0.1W_0$ and isolated thin lines without the k periodicity located roughly at $0.1W_0 \lesssim |E - FX| \lesssim 0.35W_0$ are due to the edge states. Scattered points seen around $E - FX \approx 0$ are due to the hybridized states of the central two subbands. For fixed k, there are four ($q = 4$) main energy branches, and some edge states. This diagram is very similar to the one at $F = 0$, which is shown in Fig. 3.5, in the sense that there are four subbands in similar shapes with the periodicity with respect to k. The reason why the eigenenergy for $F \neq 0$ is similar to the one for $F = 0$ is understood in the following way. For appropriately strong field such that V is larger than the subband width at zero electric field, the eigenenergy is characterized by q sets of the Stark ladders, for which the energy spacing is, as will be discussed in the next section, given by $\Delta E = Fq/d$, and $X \approx q\nu/d$ with ν an integer. This implies that for fixed k, q different values of $E - FX$ correspond to the band centers of q magnetic subbands. The $F = 0$ bands have several different features, however. The energy widths $E - FX$ of each of the q subbands are broadened for $F = 0$ because of the wave vector corresponding to the freedom in the ξ direction, and absence of the hybridized states and the edge states which are caused by the electric field. The narrowing of $E - FX$ for $F \neq 0$ is caused by the electric field, which destroys the periodicity along the electric field, and kills the wavevector dependence along the field direction.

So far we have considered the case where the electric field is applied parallel to

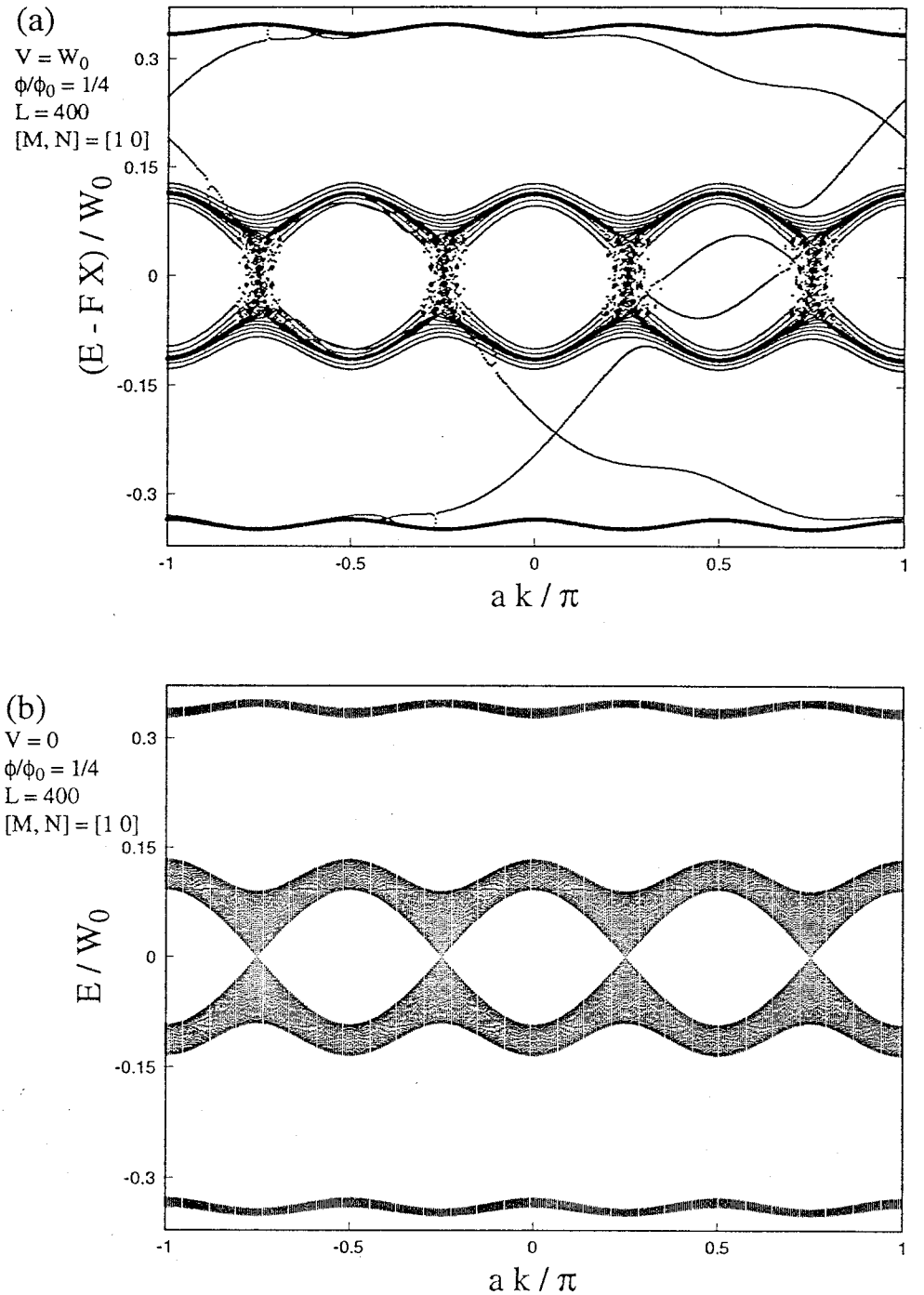

Figure 3.4: $E - FX$ as a function of k for (a) $V = W_0$ and (b) $V = 0$, where X is the gravity center of the wavefunction and k the wave number perpendicular to the electric field direction. The electric field is applied in the direction of crystal axis, *i.e.*, $[M, N] = [1\ 0]$.

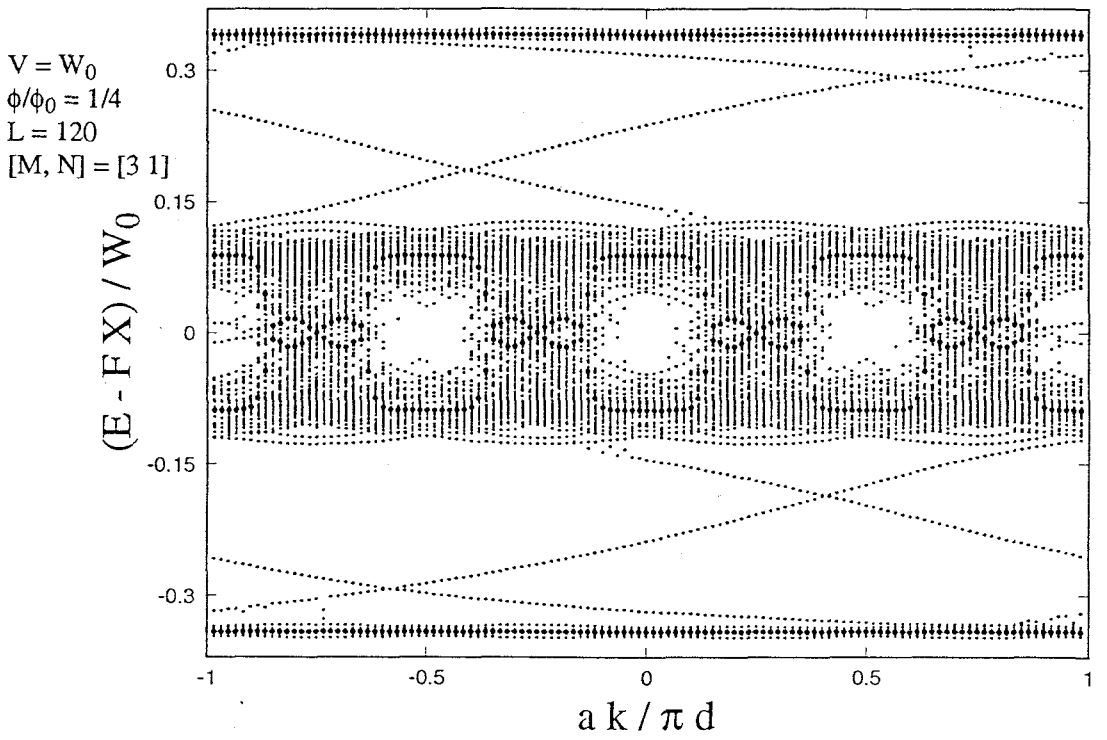

Figure 3.5: $E - FX$ as a function of k for $[M, N] = [3\ 1]$, where X is the gravity center of the wavefunction and k the wave number perpendicular to the electric field direction. The range of k is from $-\pi d$ to πd where d is the distance between the nearest net lines along the electric field.

the symmetry axis of the lattice, viz., $[M, N] = [1\ 0]$. Now we examine the case where the direction of the electric field is tilted so that the direction is parallel to $[M, N]$ with $MN \neq 0$. We have checked that the density of states and the functional dependence of E/W_0 on X are almost unchanged from the case of [1 0]. The main and important effect of the tilting of the electric field is to freeze partly the dispersion with respect to k (see Eq. (3.7)). In order to show this, the energy $(E - FX)/W_0$ against k for this case is plotted in Fig. 3.5. The eigenenergies $E - FX$ are symmetric with respect to the origin $E - FX = 0$ and $k = 0$. The top and the bottom subbands are located roughly at $(E - FX)/W_0 \simeq \pm 0.34$, which show no k dispersion. The states denoted by the round dots without k dispersion (*i.e.* $(E - FX) \simeq 0.088W_0$) are Stark localized. The round dots belonging to the central subband keep the periodicity $\Delta k = 2\pi d/q$ with respect to k. The reason for this periodicity will be discussed in the next section. Round dots have the multiplicity $\simeq L/qd$ and square dots have no multiplicity of energy. Round dots with k dispersion in the $E - FX \lesssim 0.03W_0$ denote the hybridized states of the two magnetic subbands of the zero electric field. This is because two central subbands touching together [33,58] at zero electric field easily form a single wider band by applying the electric field and the mixing of the wavefuntions becomes appreciable. The square dots are due to the edge states and the number of the states is negligibly small as compared to the number of the bulk states. The fact that bulk of the wavefunctions for a fixed k belongs to four $(q = 4)$ different eigenenergies can be contrasted to the case of $\phi = 0$. In the latter, most of the eigenenergies are dispersionless with respect to k and are given by a single energy value $E - FX = 0$ [53], since the hopping of electrons onto the nearest neighbor lattice sites for $\phi = 0$ are prohibited because of the energy difference generated by the electric field.

3.4 The Symmetries of the Model

In order to understand the behavior of $E - FX$ in Fig. 3.5, we rewrite (3.8) in the following way

$$(H_0 + F\xi)C_k(\xi) = EC_k(\xi), \tag{3.10}$$

where H_0 is the Hamiltonian in the magnetic field:

$$\begin{aligned} H_0(\xi; k, \phi) = \; & -2t \left[\cos\{Md(k - 2\pi\phi\xi) - iNd(\partial/\partial\xi)\}\right. \\ & + \left. \cos\{Nd(k - 2\pi\phi\xi) + iMd(\partial/\partial\xi)\}\right]. \end{aligned} \tag{3.11}$$

The Hamiltonian $H_0(\xi; k, \phi)$ has the following symmetry properties:

$$H_0(\xi + q/d; k, p/q) = H_0(\xi; k, p/q), \tag{3.12}$$

$$H_0(\xi + d; k - 2\pi pd/q, p/q) = H_0(\xi; k, p/q). \tag{3.13}$$

The first property implies that H_0 is periodic in ξ with periodicity q/d. From the second property and the standard argument of the magnetic translation operator [55], the size of the reduced Brillouin zone is given by $\Delta k = 2\pi d/q$. For zero electric field, the eigenenergies are split into q subbands by the magnetic field. When both of the electric and magnetic fields are applied, the eigenstates of $H_0(\xi; k, p/q) + F\xi$ is given by the Stark ladder states with the energy spacing given by $\Delta E_\alpha(k, p/q) = Fq/d$ for an infinite lattice where α is the subband index. This implies that the wavefunctions corresponding to the Stark ladders are localized near $X \approx q\nu/d$ with ν an integer. Consequently, the energy spectrum $E - FX$ is less influenced by the electric field and has almost the original character of the subbands for the zero electric field. This explains the periodicity of $E - FX$ with respect to k in Fig. 3.5.

3.5 Summary of Chapter 3

In this chapter, electronic states of the two-dimensional tight-binding model are studied when both uniform electric and magnetic fields are present. It is shown that the Stark ladder states are observed associated with each of the magnetically induced subbands for a high electric field $F \gtrsim W_0/L$. The Stark ladder spacing is given by Fq/d where $d = (M^2 + N^2)^{-1/2}$ and $\phi/\phi_0 = p/q$ with $[M, N]$ the direction of the electric field. For the symmetric direction, *i.e.*, $[M, N] = [1\ 0]$, the eigenenergies have the dispersion with respect to the wave vector k perpendicular to the electric field, but for the general non-symmetric direction such that $MN \neq 0$, this k dispersion is killed and the eigenenergies become k independent. Irrespectively of the electric field direction, the density of states becomes the pyramid shape with q steps when the electric potential drop V through the system becomes comparable to the original bandwidth of the zero field.

Chapter 4

The Ballistic Transport in Crossed Electric and Magnetic Fields

The nature of the ballistic transport properties on the two–dimensional lattice in applying the electric field in the axis direction and magnetic fields normal to the plane is investigated. The electric fields makes the electron wave functions localized on the narrow channels perpendicular to the electric field and the conductance quantization through these narrow channels is expected to occur. A tight–binding Hamiltonian which is employed to describe the system which is connected with perfect leads. Numerical computations are performed on the basis of the two–terminal Landauer formula for the conductance with the transmission coefficients in the perpendicular direction to the strong electric field calculated from the recursive Green's function technique.

4.1 Introduction to Chapter 4

The conductance through the narrow channels has been studied experimentally [61, 62] and theoretically [63–65]. Recently the suitable sample for the "point contact" is fabricated at the GaAs–AlGaAs interface of the heterostructure. The schematic top view was given in Fig. 4.1a, while the Fig. 4.1b shows a cross–sectional view of the split gate. By applying a negative voltage to a split gate, electrons on the large two dimensional regions under the gates are depleted, leaving a narrow channel in which electrons are undepleted. In this way one can define short and small region where two–dimensional electron gas exists with variable width $0 \lesssim W \lesssim 250$nm comparable to the Fermi wavelength (≈ 40nm) and much shorter than the mean free path ($\approx 10\mu$m). This is the "quantum point contact". The length of the contact also much shorter than the mean free path, and hence the transport is ballistic. Van Wees *et al.* [61] and Wharam *et al.* [62] independently discovered a sequence of steps in the conductance of such a point contact when its width was varied by means of the voltage on the split gate. The steps are close to integer multiples of $2e^2/h$.

The ballistic transport in the point contact is studied theoretically [63] based on the Landauer formula [66,67]. Consider an ideal two–dimensional conductor without impurities or inhomogeneties of width connecting two electron reservoirs as shown in Fig. 4.2. The electron reservoirs at chemical potentials μ_1 and μ_2 serve as source and sink of carriers and of energy. One reservoir emits carriers into current–carrying states up to its chemical potential. Every carrier reaching either the other or the original reservoir, independent of phase and of energy, is absorbed without reflection.

The Hamiltonian of the perfect conductor is

$$H = \frac{1}{2m}(p_x^2 + p_y^2) + V(x), \tag{4.1}$$

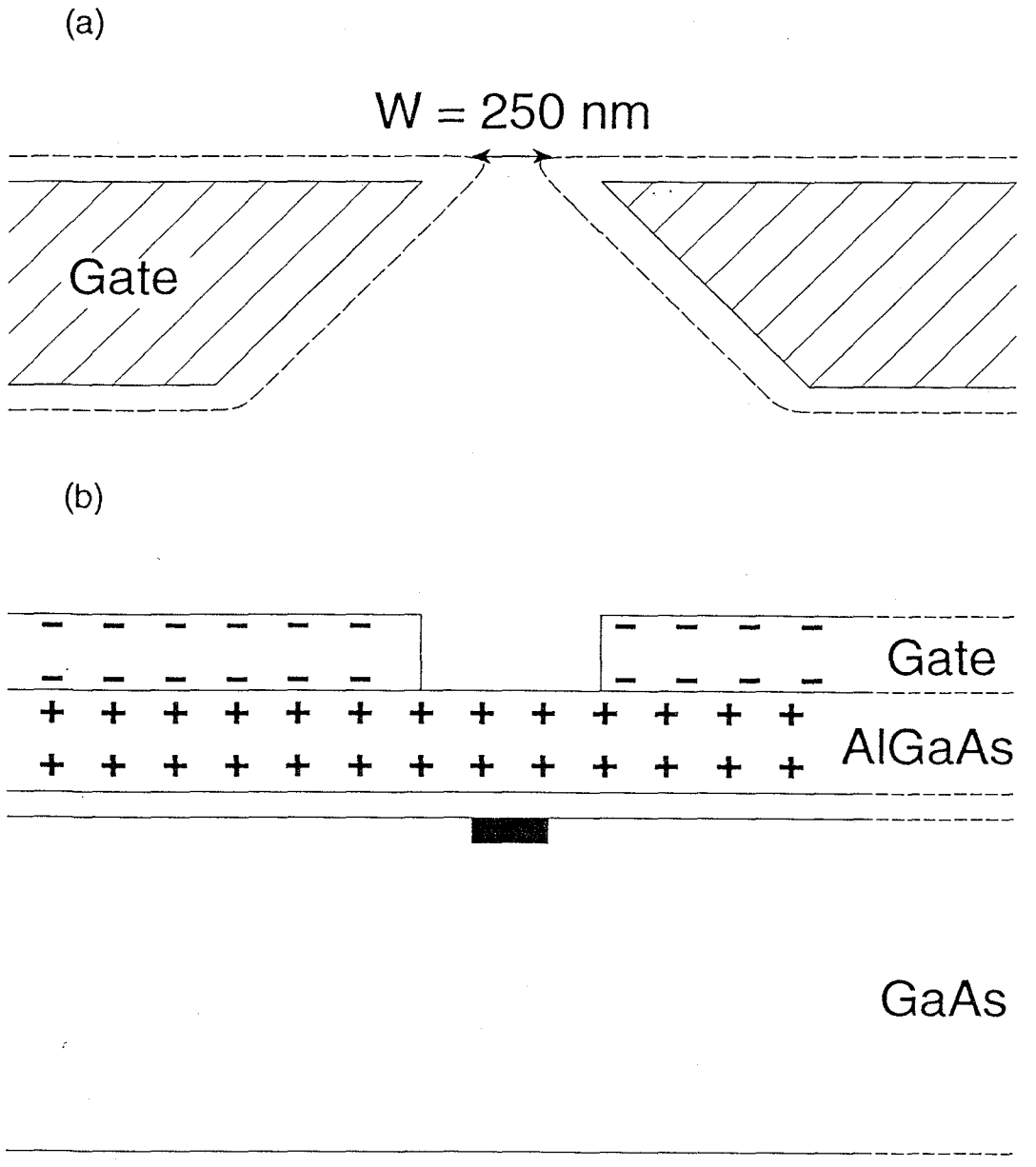

Figure 4.1: The schematic top (a) and cross-sectional (b) view of the split gate. By applying a negative voltage to a split gate indicated by the hatched regions, electrons under the split gates are depleted, leaving a narrow channel represented by the black square region in which electrons are undepleted. Positive ionized donors in AlGaAs and negative charges on a Schottky gate electrode are indicated.

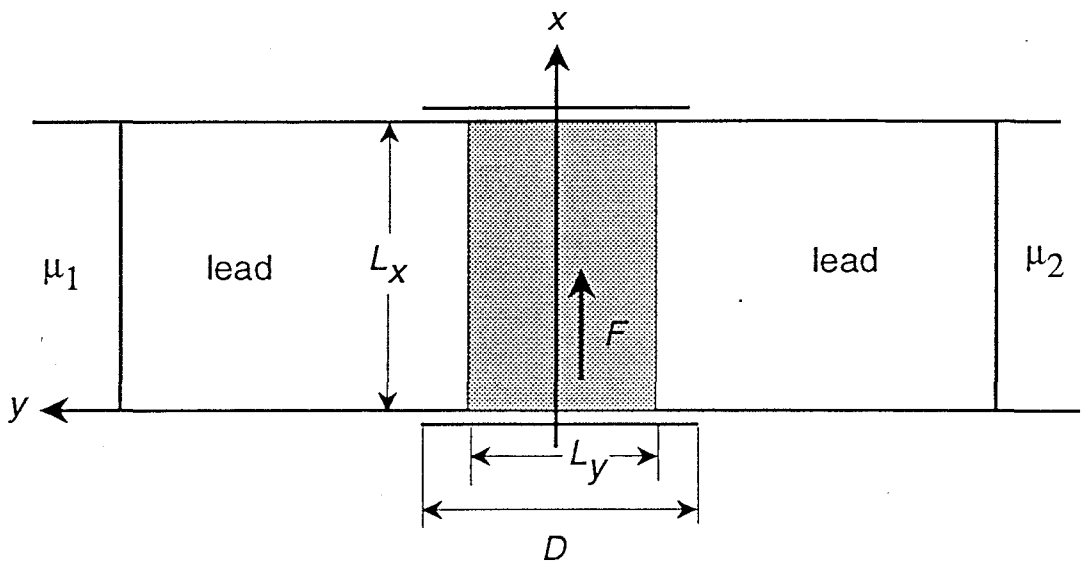

Figure 4.2: The electric potential F produced by the condenser plates. The sample occupies the region $0 < x < 20, -10 < y < 10$, which is shown by shadow. The condenser plates with width $D = 52$ are located at $x = 0$ and 20. The leads are attached both side of the sample, which is connected the heat reservoirs. The chemical potential μ_1 and μ_2 of the heat reservoirs are slightly different each other and $\mu_1 < \mu_2$. The magnetic field is applied perpendicular to the plane.

where y is the coordinate along the strip, x the coordinate transverse to the strip and $V(x)$ the confining potential. The wavefunctions are separable and of the form

$$\varphi_{j,k}(x,y) = \mathrm{e}^{iky} f_j(x), \tag{4.2}$$

where k is the wavevector along y and $f_j(x)$ a transverse eigenfunction with energy eigenvalue E_j. The total energy of the state is the sum of the transverse (x–direction) energy E_j and the energy for longitudinal (y–direction) motion. Thus at the Fermi energy $E_F = E_j + \hbar^2 k_j^2/2m$, there are $2N$ states, where N is the number of transverse energy E_j below the Fermi energy. Let us calculate the current through this perfect conductor assuming $\mu_1 < \mu_2$. Below μ_1 left– and right–moving states are equally occupied, and the net current is zero. Thus we need to be concerned only with those

states the energy of which is located between μ_1 and μ_2. The current injected from the right reservoir in the channel j is $I_j = ev_j(dn/dE)_j\Delta\mu$, where $v_j = \hbar^{-1}(dE_j/dk)$ is the longitudinal velocity at the Fermi energy of the channel j. $(dn/dE)_j$ is the density of states at the Fermi energy for this channel and $\Delta\mu = \mu_2 - \mu_1$. In one dimensional system the density of states is $(dn/dE)_j = 1/2\pi\hbar v_j$ since $dn/dk = 1/2\pi$. Therefore, the current fed into a channel is

$$I_j = (e/h)\Delta\mu, \tag{4.3}$$

independent of the channel index j. The total current is $I = N(e/h)\Delta\mu$. The voltage drop between the reservoirs is $eV = \Delta\mu$, and thus the conductance of a perfect N–channel wire is

$$G = \frac{e^2}{h}N. \tag{4.4}$$

When the magnetic field is applied to the point contact, the dispersion relation is modified, and we have bulk Landau levels and magnetically induced edge states. The quantization (4.4) is still true for this case, because the fundamental cancellation of the group velocity $v_j = \hbar^{-1}(dE_j/dk)$ and the density of states in the one dimensional system $(\pi\ dE_j/dk)^{-1}$ holds regardless of the form of the dispersion relation $E_j(k)$ of the states located near the both system edges which is parallel to the flow. In this case the magnetic edge channels at the Fermi level take over the role of one dimensional subbands. Thus, the right going electrons and the left going electrons is separated spatially. The above discussion for the pure case gives a hint for the dirty case. When there are impurities in the sample, the spatial separation between the right– and the left–going channels due to the magnetic field reduces the reflection. Thus, even in the presence of impurities, the plateau of the conductance reflecting the perfect transmission survives in the magnetic fields [68].

We give a different kind of the point contact, *i.e.*, the narrow strip is fabricated by the strong electric field in two dimensional plain. When an strong electric field is applied in the lattice plane and we assume the infinitely high potential walls at the perpendicular boundaries to the field, the wavefunction is localized in the bulk parallel to the electric field, and moreover, the wave functions are confined around the system edges because in the vicinity of the lattice edges the triangular potential is formed by the electric field [56]. Such wave functions are localized in the parallel direction while they are plane wave like in the perpendicular direction, producing narrow channels perpendicular to the field. In the narrow channels the electron move freely in the perpendicular direction to the field. We may expect that the conductance is also quantized in our model. We present in this chapter the calculations of the conductance through this narrow channels induced by strong electric fields.

When both the electric and magnetic fields are applied, the change of the plateaux of the conductance by the magnetic field is presented. The electronic energy states in the two–dimensional tight–binding model in the magnetic field applied normal to the lattice plane is known to be fairly complex as discussed in the previous chapters [33]. When the normalized magnetic field ϕ/ϕ_0 is equal to the rational number p/q, where ϕ is the magnetic flux through the unit cell, $\phi_0 = ch/e$ the flux quantum and p and q are integers prime to each other, the energy eigenstates are split into q subbands. Wave functions for this system are extended over the entire lattice. This behavior is very different from those in the case of free electrons, where the Landau states are localized around the centers of the circular motion and their energies are all degenerate for the fixed Landau index. For a finite system with confining walls, the electron states near the boundaries are appreciably modified, and the electrons

migrate on the classical skipping orbits at both edges of the system [69–72]. It is expected that the edge states contribute the transfer, *i.e.*, edge channel is appeared. The width of each channel is roughly equal to the magnetic length $\{\phi_0/(2\pi\phi)\}^{1/2}$ in units of the lattice constant.

As we see in the previous section, the eigenstates in both the electric and magnetic fields have the peculiar feature. When the moderate electric field is applied, each magnetic sub–band becomes the Stark ladder bands. Their wavefunctions are localized in the electric field direction, and hence there are many strips in space the number of which is equal to the number of the original magnetic sub–band. These strips are also the candidate of the channel. When the electric field becomes further stronger, the eigenvalue is shown to form the single band of the Stark ladder.

When there are impurities in the sample, it is expected that the quantization of the conductance will be broken by the electric field due to the enhancement of the backward scattering, *i.e.*, the transport is ballistic at zero electric field and diffusive at high electric field case. In the intermediate electric field the transport properties are not clear. Therefore, we study the transition of the conductance from the ballistic to the diffusive regime in this chapter.

The organization of this chapter is the following. In Section 4.2 we given the model for the crossed electric and magnetic field. In Section 4.3 the conductance as the function of the electric field is shown for the various magnetic fields. The conclusion of this chapter is given in the final section.

4.2 Model and Method

The arrangement of the model for the numerical calculation is shown in Fig. 4.2. We consider the 2D lattice of dimensions $L_x \times L_y$ (the lattice constant is set to be unity) and assume that the electric field is applied along the x direction by the condenser plates with width D at $x = 0$ and L_x, and the magnetic field is applied parallel to the z direction. The condenser width D is taken to be a little bit larger than L_y so that the effective potential along the y direction in the sample becomes linear. The probes to measure the conductance are attached at $y = \pm Y$ where Y is much larger than the sample width L_y. The effective electric potential in the system is determined by the Laplace equation with the boundary conditions where the electric potential is zero at $x = 0$ and $y = \pm Y$, and is equal to $V = FL_x$ for $x = L_x$ and $|y| < D/2$ with F the electric potential drop across a unit cell. The resultant electric potential near the sample is shown in Fig. 4.3 for $L_x = L_y = 20$, $D = 52$ and $Y = 677$.

In order to consider the electric flow in the magnetic field, the effect of the Coulomb interaction is crucial [73,74]. It is assumed, however, that the Hall voltage is negligible because the transport in the electric field direction is insulating due to the Stark ladder. The validity of this assumption is discussed in the Appendix A.

The Schrödinger equation for the sample with random impurities is given by the following tight-binding model:

$$-t\left\{C(x+1,y)+C(x-1,y)+C(x,y+1)\mathrm{e}^{2\pi i(\phi/\phi_0)x}+C(x,y-1)\mathrm{e}^{-2\pi i(\phi/\phi_0)x}\right\}$$
$$+FxC(x,y)+U(x,y)C(x,y)=EC(x,y), \tag{4.5}$$

where $U(x,y)$ is the random potential and the confining walls are assumed implicitly to be located at $x = 0$ and L_x. The corresponding boundary conditions for $\psi(x,y)$ are given by $\psi(0,y) = \psi(L_x,y) = 0$. For the calculation of the conductance, $\psi(x,+Y)$ is

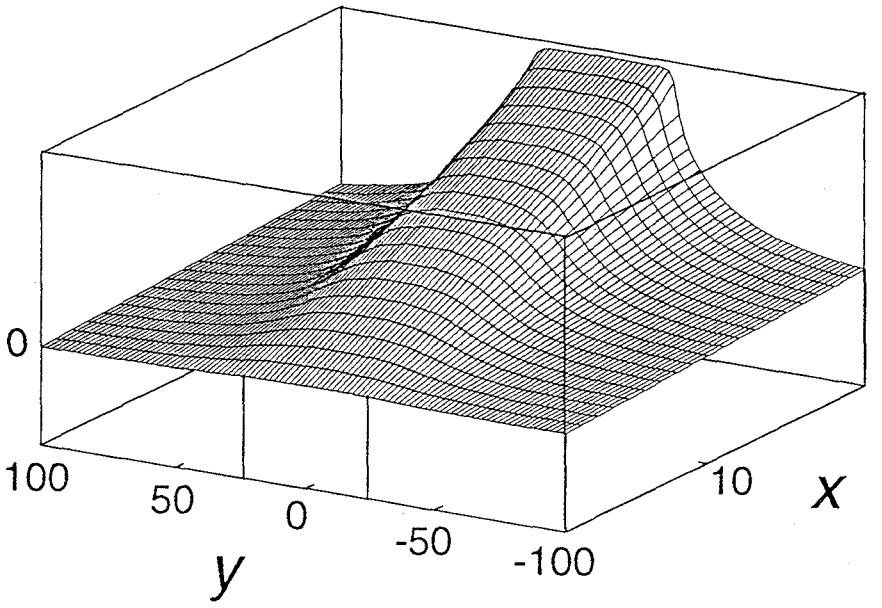

Figure 4.3: The effective electric potential in the neighborhood of the sample. The sample occupies the region $0 < x < 20$, $-10 < y < 10$, and the applied voltage along the x axis is $V = 0.6\ t$ where t is the transfer energy. The condenser plates with width $D = 52$ is located at $x = 0$ and 20.

connected with the incident and reflected waves within the probe and $\psi(x, -Y)$ with the transmitted waves. The conductance along the y axis is evaluated as a function of the Fermi energy based on the Landauer formula [66,67] from the transmission coefficients which are calculated by the recursion method proposed by Ando [65]. The recursion method is the strictly expansion of the Landauer formula to the two-dimensional tight-binding model reviewed in the Appendix B.

4.3 Transport of the 'quantum wire'

First we show the conductance calculated as a function of the electric field F, which is shown in Fig. 4.4. Here the strength of the incident energy of the electron at the probe $y = -Y$ is fixed to be $E_F = 1.6t$ and the sample size is $L_x = L_y = 20$. The conductance for the case without the random potential is plotted by thin lines and for the case with the random potential by thick lines. The strength of the random potential is distributed between $-t/2$ and $+t/2$ with the flat probability distribution. We calculate the conductance of 1000 different samples and the mean value of conductance is plotted by the thick line and the standard deviation is given by the error bars.

The Fig. 4.4a shows the case without magnetic field, where the conductance for the pure case shows a step–like feature with its plateau quantized in units of $2e^2/h$. This is because electrons move freely along the channel with wave vector k and the conductance for such a case is known to be quantized [63]. The step width ΔF for $E_F \lesssim 3t$ reflects the energy difference of the quantized edge states, the wave functions of which are approximated by the Airy functions Eq. (1.10) [14]. When the random potential is introduced into the sample, the conductance for fixed E_F becomes smaller than the one for the pure case, and the steps become corroded, so that the step–like feature of the conductance becomes unclear. The reason for the decrease of the conductance for the impure case, *i.e.*, the increase of the backward scattering, is that the impurities make the wave function localized in the y direction and mix the forward–going and backward–going waves and hence the transmission probability decreases.

When the magnetic field is applied, the conductance for the pure sample also shows a step–like feature with its plateau quantized in units of $2e^2/h$ as shown in

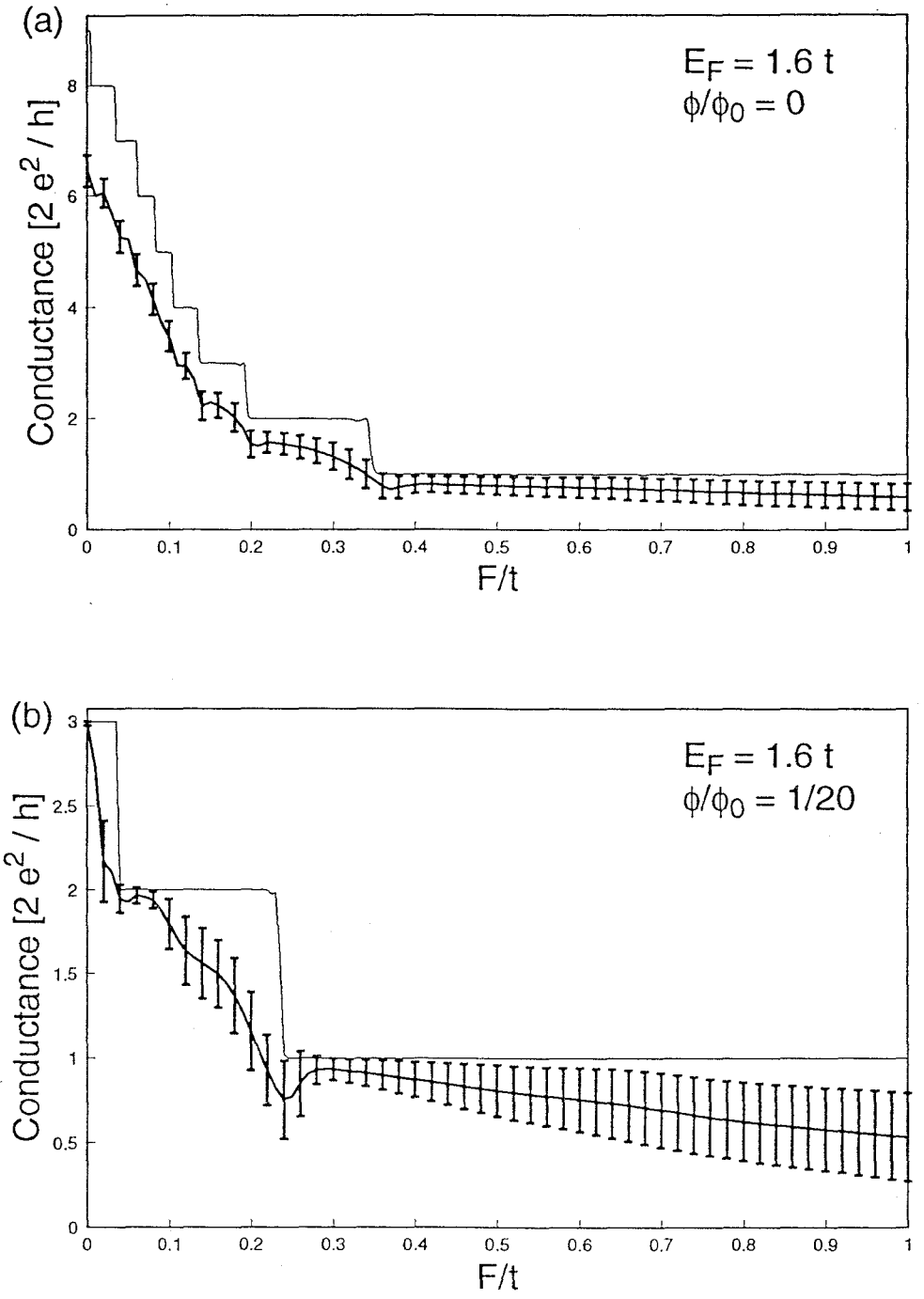

Figure 4.4: The electric field dependence of the conductance for (a) $\phi/\phi_0 = 0$ and (b) $\phi/\phi_0 = 1/20$. Thin lines show the case without the random potential and thick lines show the case without the random potential. Error bars are estimated from 1000 different samples.

Fig. 4.4b. and the step width is now estimated from the cyclotron energy separation. This quantization comes from the fact that the wave function along the y direction is still characterized by the wave vector k [69]. This indicates that the electrons move freely along the y direction, and therefore the conductance is quantized. The most noticeable effect of the magnetic field is to reduce the number of plateaux in a given electric field. This provides a demonstration of depopulation of magnetoelectric subbands. In addition, one observes that the reduction of the conductance from the plateaux of the pure case improves in the presence of the random potential compared to the case without magnetic fields. This is due to the reduction of the reflection probability at the sample, which is shown in the dirty sample on the absence of magnetic field. This is because the location of the wave functions of the forward–going and the backward–going waves are separated spatially by the distance $\sim E_G/F$, where E_G is the bandgap between magnetically induced subbands, so that the mixing of these waves are reduced as compared to the case of vanishing magnetic field. In other words, the application of the magnetic field favors the conductance quantization.

4.4 Conclusion of Chapter 4

We have examined the conductance quantization of the narrow channels which are realized by the application of both electric and magnetic fields. For pure samples, the conductance quantization is clearly seen, and the step width ΔF reflects the energy separation between the Airy edge states for the case of the electric field only, or that between the cyclotron energy separation for the case where both electric and magnetic fields are applied. In the dirty samples, the conductance quantization is severely damaged for the case where only the electric field is present. In contrast, the quantization is only partly destroyed when both of the electric and magnetic fields are applied, *i.e.*, the quantization of the conductance is more easily observable by the application of the magnetic field.

Appendix A

The Effects of the Hall Voltage

In order to consider the electric flow in the magnetic field, the effect of the Coulomb interaction is crucial [73]. In the steady states the Lorentz and Coulomb forces cancel out each other. The electrostatic potential in the sample between the condenser plates has to be calculated from the local density distribution of the electron and the Coulomb interaction. In the center of the sample as the effects of the edges of the condenser plates are negligible, the electron system may treat as the infinite wires which are parallel to the condenser plates. The Schrödinger equation (1.17) is modified as

$$-t\left[\psi_{x+1}(k)+\psi_{x-1}(k)\right]+V(x)\psi_x(k)=E\psi_x(k), \tag{A.1}$$

$$V(x)=2\cos\left(2\pi\frac{p}{q}x+k\right)+Fx-\sum_{x'\neq x}D\lambda(x')\log|x-x'|, \tag{A.2}$$

where $D=e^2/2\pi\epsilon a$ with ϵ the dielectric constant and the local density of the electron is written as

$$\lambda(x')=\frac{1}{L_x}\sum_{E<E_F}|\psi_{x'}(k)|^2, \tag{A.3}$$

where the summation is taken in such a way that the states are below the Fermi level E_F. We calculate $V(x)$ from Eq. (A.2) with the boundary conditions

$$V(0)=0, \tag{A.4}$$

$$V(L_x)=V, \tag{A.5}$$

and determine F and the local density of the electron self-consistently.

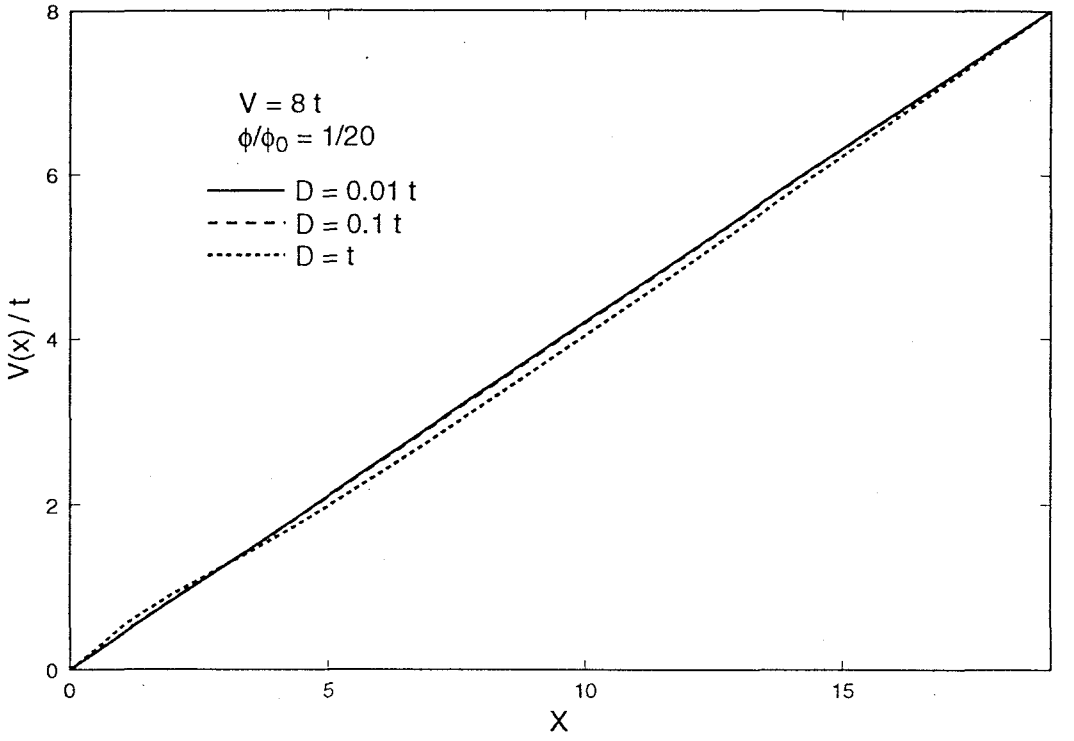

Figure A.1: The electrostatic potential in the sample as the function of x, which is calculated with the local density distribution of the electron and the Coulomb interaction.

We calculate numerically under the condition that the magnetic field $p/q = 1/20$ is fixed and $V = 8t$. The result is shown in Fig. A.1, where the potential $V(x)$ is plotted. In the quantum dot lattice system the lattice constant is of the order of μ m, and if we take the dielectric constant $\epsilon = 12.9$ of the bulk GaAs, then we get $D \sim 0.2$ [meV]. As the dielectric constant and the lattice constant in the quantum dot lattice depends on each sample we calculate three case, *i.e.*, the large dielectric constant case ($D = 0.01t$), the middle ($D = 0.1t$) and the small ($D = t$) where t is estimated as the order of meV.

The effect of the re–distribution of the electron and Coulomb force is negligible in our model. The re–distribution of the electron is small in our calculation because in

the Stark ladder states the system is insulator in the field direction. In the quantum dots lattice as the lattice constant is sufficiently larger than the normal material, the effect of the Coulomb interaction is negligible. The effective electrostatic potential is nearly linear.

Appendix B

Recursion Formula

In this appendix the numerical technique for calculating the conductance introduced by Ando [65] is reviewed. First we shall consider a two–dimensional wire infinitely long in the y direction and consisting of L_x lattice sites in the x direction. The Schrödinger equation of the tight–binding model of a square lattice is given as

$$(E\mathbf{I} - \mathbf{H}_0)\Phi_y + t\mathbf{P}\Phi_{y-1} + t\mathbf{P}^*\Phi_{y+1} = 0, \tag{B.1}$$

where Φ_y is a vector describing the amplitudes of the yth cell consisting of L_x sites and $\mathbf{P}$ is an $L_x \times L_x$ matrix consisting of phase factors

$$\{\mathbf{P}\}_{x,x'} = \exp\{-2\pi i(\phi/\phi_0)x\}\delta_{x,x'}, \quad (x, x' = 1, \ldots, L_x). \tag{B.2}$$

The Hamiltonian $\mathbf{H}_0$ is also an $L_x \times L_x$ matrix given by

$$\{\mathbf{H}_0\}_{x,x'} = 4t\delta_{x,x'} - t(\delta_{x,x'+1} + \delta_{x,x'-1}), \quad (x, x' = 1, \ldots, L_x). \tag{B.3}$$

To obtain linearly independent solutions for Eq. (B.1) we first set

$$\Phi_y = \lambda^y \Phi_0. \tag{B.4}$$

The eigenvalue problem of (B.1) is rewritten as

$$\lambda \begin{pmatrix} \Phi_y \\ \Phi_{y-1} \end{pmatrix} = \begin{pmatrix} t^{-1}\mathbf{P}(\mathbf{H}_0 - E\mathbf{I}) & -\mathbf{P}^2 \\ \mathbf{I} & \mathbf{0} \end{pmatrix} \begin{pmatrix} \Phi_y \\ \Phi_{y-1} \end{pmatrix}. \tag{B.5}$$

If $|\lambda| < 1$, then from Eq. (B.4) the solution is exponentially decaying in the positive y–direction and describes right–going evanescent modes. The solutions with $|\lambda| > 1$

describe left-going evanescent modes. If the absolution value of λ is unity then the classification is done according to the sign of the matrix element of the current density operator

$$\begin{aligned} j &= \frac{e}{2i\hbar}\left[\mathbf{\Phi}_y^\dagger \mathbf{\Phi}_{y+1} - \mathbf{\Phi}_y \mathbf{\Phi}_{y+1}^\dagger + \mathbf{\Phi}_{y-1}^\dagger \mathbf{\Phi}_y - \mathbf{\Phi}_{y-1}\mathbf{\Phi}_y^\dagger\right] \\ &= \frac{2e}{\hbar}|\mathbf{\Phi}_y|^2 \mathrm{Im}\lambda. \end{aligned} \tag{B.6}$$

If $\mathrm{Im}\lambda > 0$ then $j > 0$ and the wave is propagating to the right, and if $\mathrm{Im}\lambda < 0$ then it is propagating to the left. The equation (B.5) has $2L_x$ eigenvalues and $2L_x$ eigenvectors, which are classified into L_x right- and L_x left-going waves. Let $\mathbf{u}_1(-), \ldots, \mathbf{u}_{L_x}(-)$ be Φ_0 of the left-going solutions corresponding to $\lambda_1(-), \ldots, \lambda_{L_x}(-)$ and $\mathbf{u}_1(+), \ldots, \mathbf{u}_{L_x}(+)$ be Φ_0 of the right-going solutions corresponding to $\lambda_1(+), \ldots, \lambda_{L_x}(+)$. Define the matrices

$$\mathbf{U}(\pm) = [\mathbf{u}_1(\pm) \cdots \mathbf{u}_{L_x}(\pm)], \tag{B.7}$$

and

$$\{\mathbf{\Lambda}(\pm)\}_{x,x'} = \lambda_x(\pm)\delta_{x,x'} \quad (x, x' = 1, \ldots, L_x). \tag{B.8}$$

Any left- and right-going waves are written at $y = 0$ as

$$\mathbf{\Phi}_0(\pm) = \mathbf{U}(\pm)\mathbf{\Phi}(\pm), \tag{B.9}$$

where $\mathbf{\Phi}(\pm)$ is an appropriate vector consisting of expansion coefficients. For general y we have

$$\mathbf{\Phi}_y(\pm) = \mathbf{U}(\pm)\mathbf{\Lambda}(\pm)^y \mathbf{\Phi}(\pm), \tag{B.10}$$

which leads to the relation

$$\mathbf{\Phi}_y(\pm) = \mathbf{F}(\pm)^{y-y'} \mathbf{\Phi}_{y'}(\pm), \tag{B.11}$$

with

$$\mathbf{F}(\pm) = \mathbf{U}(\pm)\mathbf{\Lambda}(\pm)\mathbf{U}^{-1}(\pm). \tag{B.12}$$

For the purpose of transport calculations the quantum wire is sandwiched between two perfect leads. We define our lead–sample–lead system to lie along the y–axis as show in Fig. 4.2. It can be divided into slices along that direction, each of which has L_x sites, *i.e.*, a cross–section of the quantum wire. Now let us consider the scattering problem for the wire with length L_y. First, we separate the amplitude $\mathbf{\Phi}_y$ at cell y into the right–going and left–going solution:

$$\mathbf{\Phi}_y = \mathbf{\Phi}_y(+) + \mathbf{\Phi}_y(-). \tag{B.13}$$

Define the Green function $\mathbf{G}$ as

$$\mathbf{G} = \frac{1}{E\mathbf{I} - \mathbf{H}}, \tag{B.14}$$

with

$$\mathbf{H} = \begin{bmatrix} \mathbf{H}_0 - t\mathbf{P}\mathbf{F}^{-1}(-) & -t\mathbf{P}^* & 0 & \cdots & 0 & 0 \\ -t\mathbf{P} & \mathbf{H}_1 & -t\mathbf{P}^* & \cdots & 0 & 0 \\ 0 & -t\mathbf{P} & \mathbf{H}_2 & \cdots & 0 & 0 \\ \vdots & \vdots & \vdots & \ddots & \vdots & \vdots \\ 0 & 0 & 0 & \cdots & \mathbf{H}_{L_y} & -t\mathbf{P}^* \\ 0 & 0 & 0 & \cdots & -t\mathbf{P} & \mathbf{H}_{L_y+1} - t\mathbf{P}^*\mathbf{F}(+) \end{bmatrix}, \tag{B.15}$$

where the Hamiltonian $\mathbf{H}_y$ is an $L_x \times L_x$ matrix given by

$$\{\mathbf{H}_y\}_{x,x'} = (4t + \nu(x,y))\delta_{x,x'} - t(\delta_{x,x'+1} + \delta_{x,x'-1}), \quad (x, x' = 1, \ldots, L_x), \tag{B.16}$$

and $\mathbf{H}_{L_y+1} = \mathbf{H}_0$ with $\nu(x,y)$ being the local potential energy at the site (x,y). Immediately, we can derive

$$\mathbf{\Phi}_{L_y+1}(+) = -t\,(L_y + 1|\mathbf{G}|0)\,\mathbf{P}\left[\mathbf{F}^{-1}(+) - \mathbf{F}^{-1}(-)\right]\mathbf{\Phi}_0(+), \tag{B.17}$$

where $(L_y + 1|\mathbf{G}|0)$ is the Green's function which couples the 0th and the $(L_y + 1)$st slice in our system, *i.e.*, the last slice in the left–lead and the first slice in the right–lead. The Green's function $(L_y+1|\mathbf{G}|0)$ is calculated iteratively by using the recursive

method [75]. From these equations we can obtain the amplitude transmission coefficients t_{mn} for the incident channel n with velocity v_n and out–going channel m with velocity v_m as

$$t_{mn} = \sqrt{\frac{v_m}{v_n}} \left[-t\mathbf{U}^{-1}(+) \left(L_y + 1|\mathbf{G}|0 \right) \mathbf{P}[\mathbf{F}^{-1}(+) - \mathbf{F}^{-1}(-)]\mathbf{U}(+) \right]_{mn} . \qquad \text{(B.18)}$$

The conductance G is given by the multichannel version of Landauer's formula Eq. (4.4) [66,67].

$$G = \frac{e^2}{\pi\hbar} \sum_{m,n} |t_{mn}|^2 . \qquad \text{(B.19)}$$

This numerical technique has proved very reliable for the Anderson localization problem [76,77].

Chapter 5

Summary and Concluding Remarks

In this thesis, we have investigated the electronic states in the tight–binding model on the two-dimensional square lattice under the strong electric field with various direction of the electric field. It is shown that the value of the density of states in the band center region is independent of the field direction when the Stark ladder states appear, although the periodicity of the crystal along the electric field is a irregular function of the field direction, and hence the Stark ladder spacing becomes erratic. By looking at the finite lattice, we find that the edge states are characterized by the Airy spectrum and that some unexpected energy gaps appear for the appropriate electric field strength.

We also investigated Stark ladder states of the magnetic subbands, when both uniform electric field is present in the plane and the magnetic field is applied perpendicular to the plane. It is shown that the Stark ladder states are seen in each of the magnetically induced subband for a high electric field $F \gtrsim W_0/L$, where F the potential drop through the unit of the lattice, W_0 the bandwidth in the absence of the fields and L the system size. The Stark ladder spacing is given by Fq/d where $d = (M^2 + N^2)^{-1/2}$ and $\phi/\phi_0 = p/q$ with $[M, N]$ the direction of the electric field. For the symmetric direction, *i.e.*, $[M, N] = [1\ 0]$, the eigenenergies have the dispersion with respect to k, where k is the wavevector perpendicular to the electric field. For the general non–symmetric direction such that $MN \neq 0$, this k dispersion is killed and the eigenenergies become k independent. Irrespective of the electric

field direction, the density of states becomes the pyramid shape with steps when the electric potential drop through the system becomes comparable to the original bandwidth of the zero field. When the electric field F becomes extremely strong $W_0/F \ll \sqrt{2\pi q/p}$, the stark ladder states seen in each of the magnetically induced subband for the moderate electric field become Stark ladder of one band.

We have investigated the ballistic transport of the 'quantum wire' which are realized by the application of strong electric field. We examine the dependence of the random potential and magnetic fields. For pure samples, the conductance quantization is clearly seen, and the step width ΔF reflects the energy separation between the Airy edge states for the case that only the electric field is applied, or that between the cyclotron energy separation for the case where both electric and magnetic fields are applied. In the dirty samples, the conductance quantization is severely damaged for the case where only the electric field is present. In contrast, the quantization is only partly destroyed when both of the electric and magnetic fields are applied, *i.e.*, the quantization of the conductance is more easily observable by the application of the magnetic field.

It is discussed that the Stark ladder states in the two-dimensional system would have realized in the quantum dots lattice. The dots lattice is fabricated by holographic lithography in arrays on macroscopic areas. In the system the lattice spacing is controllable, and the strong field condition considered in this thesis may be fulfilled easily by experimentally accessible field strengths.

Reference

[1] G. H. Wannier: Phys. Rev. **117** (1960) 432.

[2] G. H. Wannier: Rev. Mod. Phys. **34** (1962) 645.

[3] G. H. Wannier and D. R. Fredkin: Phys. Rev. **125** (1962) 1910.

[4] J. Bleuse, G. Bastard and P. Voisin, Phys. Rev. Lett. **60** 220(1988).

[5] P. Voisin, J. Bleuse, C. Bouche, S. Gaillard, C. Alibert and A. Regreny: Phys. Rev. Lett. **61** (1988) 1639.

[6] S. Katsura, T. Hatta and A. Morita: Sci. Rep. Tohôku Imp. Univ. **34** (1950) 19.

[7] P. Feuer: Phys. Rev **38** (1952) 92.

[8] E. O. Kane: J. Phys. Chem. Solids **12** (1959) 181.

[9] H. D. Rees, J. Phys. Chem. Solids **28** (1967) 353.

[10] G. C. Stey and G. Gusman: J. Phys. **C6** (1973) 650.

[11] M. Saitoh: J. Phys. **C6** (1973) 3255.

[12] S. Maekawa, Phys. Rev. Lett. **24**, 1175, (1970).

[13] R. W. Koss and L. M. Lambert, Phys. Rev. **B 5** (1972) 1479.

[14] M. Saitoh: J. Phys. C **5** (1972) 914.

[15] W. Franz, Z. Naturforsch. Teil **A 13** (1958) 484.

[16] L. V. Keldysh, Zh. Eksp. Teor. Fiz. **34** (1958) 1138 [Sov. Phys. -JETP **7** (1958) 788.

[17] L. Esaki and R. Tsu, IBM J. Res. Dev. **14** 61(1970).

[18] E. E. Mendez, F. Agulló-Rueda and J. M. Hong: Phys. Rev. Lett. **60** (1988) 2426.

[19] J. Bleuse, P. Voisin, M. Allovon and M. Quillec, Appl. Phys. Lett. **53** 2632 (1988).

[20] I. Bar-Joseph, K. W. Goossen, J. N. Kuo, R. F. Kopf, D. A. B. Miller and D. S. Chemla, Appl. Phys. Lett. **55** 340(1989).

[21] J. Zak: Phys. Rev. Lett. **20** (1968) 1477.

[22] H. Fukuyama, R. A. Bari and H. C. Fogedby: Phys.Rev. **B8** (1973) 5579.

[23] J. E. Avron, J. Zak, A. Grossmann and L. Gunther: J. Math. Phys. **18** (1977) 918.

[24] S. Nagai and J. Kondo: J. Phys. Soc. Japan **49** (1980) 1255.

[25] D. Emin and C. F. Hart: Phys. Rev. **B36** (1987) 7353.

[26] Q. Niu, Phys. Rev. **B 40** 3652(1989).

[27] J. Leo and A. MacKinnon: J. Phys. **C1** (1989) 1449.

[28] T. Kawaguchi and M. Saitoh: J. Phys. **C3** (1991) 9371.

[29] H. Schneider, H. T. Grahn, K. von Klitzing and K. Ploog, Phys. Rev. Lett. **65** (1990) 2720.

[30] M. Nakayama, I. Tanaka, H. Nishimura, K. Kawashima and K. Fujiwara: Phys. Rev. **B44** (1991) 5935.

[31] G. Bastard, R. Ferreira, S. Chelles and P. Voisin, Phys. Rev. **B 50** (1994) 4445.

[32] I. Takana, M. Nakayama, H. Nishimura, K. Kawashima and K. Fujiwara, Res. Rev. **B 46** 7656(1992).

[33] D. R. Hofstadter, Phys. Rev. **B14**, 2239 (1976).

[34] G. H. Wannier: Phys. Stat. Sol. (b) **88** (1978) 757.

[35] G. H. Wannier, G. M. Obermair and R. Ray: Phys. Stat. Sol. (b) **93** (1979) 337.

[36] M. Y. Azbel': Soviet Phys. JETP **19** (1964) 634.

[37] D. J. Thouless, M. Kohmoto, M. P. Nightingale and M. den Nijs: Phys. Rev. Lett. **49** (1982) 405.

[38] P. Streda: J. Phys. C: **15** (1982) L1299.

[39] J. E. Avron, R. Seiler and B. Simon: Phys. Rev. Lett. **51** (1983) 51.

[40] M. Kohmoto: Ann. Phys. **160** (1985) 343.

[41] K. von Klitzing, G. Dorda and M. Pepper: Phys. Rev. Lett. **45** (1980) 494.

[42] R. E. Peierls: Z. Phys. **80** (1933) 763.

[43] J. M. Luttinger, Phys. Rev. **84** (1951) 814.

[44] W. Kohn, Phys. Rev. **115** (1959) 809.

[45] E. I. Blount, Phys. Rev. **126** 1636(1962).

[46] P. G. Harper: Proc. Phys. Soc. London A **68** (1955) 874.

[47] A. Rauh, Phys. Status Solidi **B69** K131(1974).

[48] H. Hiramoto and M. Kohmoto, Phys. Rev. **B40** 8225(1989).

[49] H. Hiramoto and M. Kohmoto, Int. J. of Mod. Phys. **6** 281(1992).

[50] K. Niizeki and A. Matsumura, Phys. Rev. **B48** 4126(1993).

[51] A. Aubry and G. André Ann. Isr. Phys. Soc. **3** 133(1980).

[52] F. Claro and Z. Barticevic: Phys. Rev. Lett. **B38** (1988) 361.

[53] T. Nakanishi, T. Ohtsuki and M. Saitoh: Physica **B184**(1993) 310.

[54] Ch. Sikorski and U. Merkt, Surf. Sci. 229 (1990) 282.

[55] E. M. Lifshitz and L. P. Pitaevskiĭ: *StatisticalPhysics, Part* 2 (Pergamon, London, 1958) §60.

[56] T. Nakanishi, T. Ohtsuki and M. Saitoh: J. Phys. Soc. Jpn. **62**(1993) 2773.

[57] T. Nakanishi, T. Ohtsuki and M. Saitoh in Proceedings of the 21st International Conference on Physics of Semiconductors, Beijing, August, 1992, edited by P. Jiang and H. – Z. Zheng: (World Scientific, Singapore, 1992) Volume 1, p. 741.

[58] M. Kohmoto: Phys. Rev. **B39** (1989) 11943.

[59] Y. Hasegawa, P. Lederer, T. M. Rice and P. B. Wiegmann, Phys. Rev. Lett. **63** (1989) 907.

[60] Y. Hasegawa, Y. Hatsugai, M. Kohmoto and G. Montambaux, Phys. Rev. **B41** (1990) 9174.

[61] B. J. van Wees, H. van Houten, C. W. J. Beenakker, J. G. Williamson, L. P. Kouwenhouven, D. van der Marel, and C. T. Foxon, Phys. Rev. Lett. **60** (1988) 848.

[62] D. A. Wharam, T. J. Thornton, R. Newbury, M. Pepper, H. Ahmed, J. E. F. Frost, D. G. Hasko, D. C. Peacock, D. A. Ritchie, and G. A. C. Jones, J. Phys. **C21** (1988) L209.

[63] M. Büttiker, Phys. Rev. **B38** (1988) 9375.

[64] Y. Avishai and Y. B. Band, Phys. Rev. **B40** (1989) 12535.

[65] T. Ando, Phys. Rev. **B44** (1991) 8017.

[66] R. Landauer, IBM J. Res. Dev. **1** (1957) 223.

[67] R. Landauer, Philos. Mag. **21** (1970) 863.

[68] B. J. van Wees, L. P. Kouwenhouven, H. van Houten, C. W. J. Beenakker, J. E. Mooij, C. T. Foxon, and J. J. Harris, Phys. Rev. **B38** (1988) 3625.

[69] B. I. Halperin, Phys. Rev. Lett. **57** (1982) 2185.

[70] A. H. MacDonald and P. Středa, Phys. Rev. **B29** (1984) 1616.

[71] A. H. MacDonald, Phys. Rev. **B29** (1984) 6563.

[72] L. Smrčka, J. Phys. **C17** (1984) L63.

[73] A. H. MacDonald, T. M. Rice and W. F. Brinkman, Phys. Rev. **B28** (1983) 3648.

[74] T. Suzuki and T. Ando, J. Phys. Soc. Jpn **62** (1993) 2986.

[75] A. MacKinnon, Z. Phys. 59 (1985) 385.

[76] A. MacKinnon and B. Kramer, Phys. Rev. **B47** (1981) 1546.

[77] C. M. Soukoulis, I. Webman, G. S. Grest and E. N. Economou', Phys. Rev. **B26** (1982) 1838; A. D. Zdetsis, C. M. Soukoulis, E. N. Economou and G. S. Grest, Phys. Rev.**B32** (1985) 7811.